

UC Merced

UC Merced Electronic Theses and Dissertations

Title

Nanotribology of MoS₂ Investigated via Atomic Force Microscopy

Permalink

<https://escholarship.org/uc/item/81w1n63p>

Author

Acikgoz, Ogulcan

Publication Date

2020

Peer reviewed|Thesis/dissertation

UNIVERSITY OF CALIFORNIA, MERCED

**Nanotribology of MoS₂ Investigated via Atomic
Force Microscopy**

A Thesis submitted in partial satisfaction of the requirements for the degree of
Master of Science

in

Mechanical Engineering

by

Ogulcan Acikgoz

Committee in charge:

Professor Mehmet Z. Baykara, Chair

Professor Ashlie Martini

Professor Min Hwan Lee

2020

Portion of Chapter 1 © 2020 AIP Publishing

Portion of Chapter 2 © 2020 AIP Publishing

All other chapters

© Ogulcan Acikgoz, 2020

All rights are reserved.

The thesis of Ogulcan Acikgoz is approved, and is acceptable in quality and form for publication on microfilm and electronically:

Ashlie Martini

Date

Min Hwan Lee

Date

Mehmet Z. Baykara, Chair

Date

University of California, Merced

2020

Abstract

Nanotribology of MoS₂ Investigated via Atomic Force Microscopy

Ogulcan Acikgoz

M.S. in Mechanical Engineering

Advisor: Mehmet Z. Baykara

May 2020

The potential use of two-dimensional (2D) materials as solid lubricants in micro-and nano-scale mechanical systems draws significant attention, mainly due to the fact that liquid based lubrication schemes fail at such small length scales. Within this context, the lamellar material molybdenum disulfide (MoS₂), in the form of a single or few layers, emerges as a promising candidate for the solid lubrication of small-scale mechanical systems.

Motivated as above, this thesis focuses on the nanotribological properties of mechanically exfoliated MoS₂, explored via state-of-the-art atomic force microscopy (AFM) experiments. First, the dependence of friction force on sliding speed is investigated for single-layer and bulk MoS₂ samples. The results demonstrate that (i) friction forces increase logarithmically with respect to sliding speed, (ii) there is no correlation between the speed dependence of friction and the number of layers of MoS₂, and (iii) changes in the speed dependence of friction can be attributed to changes in the physical characteristics of the AFM probe. The direction dependence (i.e. anisotropy) of friction on MoS₂ is studied next. In particular, high-resolution AFM measurements conducted by our collaborators at McGill University lead to the direct imaging of atomic-scale ripples on few-layer MoS₂ samples, allowing to explain the various symmetries for friction anisotropy that are observed in our experiments as a function of scan size. Finally, the nanotribological properties of Re-doped MoS₂ are studied, revealing a surprising, inverse dependence of friction force on number of layers, in contradiction with the seemingly universal trend of decreasing friction with increasing number of layers on 2D materials. Attempts are made to uncover the physical mechanisms behind this striking observation by way of roughness and adhesion measurements.

In summary, the results reported in this thesis contribute to the formation of a comprehensive, mechanistic understanding of the nanotribological properties of

MoS₂ in particular, and 2D materials, in general. While the speed dependence and anisotropy results are relatively self-contained, further work needs to be conducted in order to explain the inverse layer-dependence of friction observed on Re-doped MoS₂.

Acknowledgements

Foremost, I would like to express my deep and sincere gratitude to my dear supervisor Prof. Mehmet Zeyyad Baykara, who has supported me all the time during my time at UC Merced. His advice was always a light in the time of darkness at any point in my research and professional student life. Being a student of a passionate scientist whose career is full of success was one of the best lucks in my life. He has supported me all the time, and gave me an opportunity to do world-class research. I gave a talk every year in prestigious international meetings, had a chance to collaborate with successful researchers all over the world and worked in a great project supported by a seed fund from NASA through the Merced Nanomaterials Center for Energy and Sensing (MACES). In addition to his endless support for my current and future career, I want to thank him again for his way of doing research with academic integrity. I feel it was a privilege to work with both a successful and honest scientist at the edge of knowledge.

I would like to thank the members of the Baykara Lab, namely Saima A. Sumaiya, Wai H. Oo, Mohammad Jaman, and our enthusiastic undergraduate members, Anthony Rodriguez, Marco Medina and Alejandro Sanchez for their company as friends and as respectful colleagues.

I also thank my friends that I have made during my graduate education at UC Merced for their support and fun activities we were involved in together; especially Ajay Khanna, Jacques-Ezechiele Nguessan, Abhinav Kumar, Zach Petrek, David Morgan, and Haiyang Wang. And I would like to thank my dear friends Mehmet Tavaci, Ece B. Irisoz, Sinan Celik, and Ozgur Can Ozudogru from Turkey, who have always supported me and gave me courage whenever I needed.

Finally, I want to thank each of my family members for their endless support, wisdom, and patience during my education and endless scientific activities. I would like to thank my mother for every sacrifice she has made to support my education. I wish to thank my beautiful girlfriend Serra Topcugil, for always waiting for me on the other side of the world with lots of dreams and sassy cats.

To My Beautiful Mother

Contents

Abstract	iv
Acknowledgements	vi
List of Figures	x
List of Tables	xiv
1 Introduction	1
1.1 Tribology: A Brief Summary	1
1.2 Nanotribology	2
1.3 Atomic Force Microscopy	3
1.4 Lateral Force Microscopy	4
1.5 AFM Tip Calibration	7
1.5.1 Normal Calibration	7
1.5.2 Lateral Calibration	8
1.6 Force Spectroscopy	9
1.7 MoS ₂ : Physical and Lubricative Properties	9
1.8 Outline	12
2 Speed Dependence of Friction on MoS₂	13
2.1 Speed Dependence of Friction	13
2.2 Methods and Materials	14
2.3 Effect of Thickness	15
2.4 Effect of AFM Probe Characteristics	18
3 Imaging, Spectroscopy, and Friction Anisotropy of Atomic-scale Ripples on MoS₂	21
3.1 Atomic-scale Ripples on 2D Materials and Friction Anisotropy	21
3.2 Imaging of Atomic-scale Ripples on MoS ₂	22
3.3 Three-dimensional Interaction Spectroscopy of Atomic-scale Ripples on MoS ₂	24
3.4 Friction Anisotropy on MoS ₂	25

4	Nanotribology of Re-Doped MoS₂	32
4.1	Dependence of Friction on Number of Layers	32
4.1.1	Undoped MoS ₂	33
4.1.2	Re-doped MoS ₂	34
4.2	Roughness Measurements	35
4.3	Adhesion Measurements	36
5	Summary and Outlook	38
	Bibliography	40

List of Figures

1.1	Evolution from an apparent contact area to idealized single asperity contact, such as that achieved by an AFM probe [14].	3
1.2	The first atomic force microscope invented by Gerd Binnig <i>et al.</i> at IBM Research Laboratory in Zurich [16].	3
1.3	A basic representation of the AFM setup [18].	5
1.4	A sketch of the 4-quadrant photodetector with a red laser spot at the center.	6
1.5	Schematic illustration of a friction loop, showing the forward and backward lateral force signals over one scan line, the half-width of the loop (W), and the offset value from zero (D).	7
1.6	Schematic representation of the MikroMasch TGF 11 silicon calibration grating with well-defined wedges used in the lateral calibration of all cantilevers utilized in this work [23].	9
1.7	Schematic representation of a typical force vs. distance curve.	10
1.8	The crystal structure of monolayer MoS ₂ in different views. Mo is shown in turquoise and S in yellow [39].	11
2.1	(a) Three-dimensional representation of a topographical AFM image showing the multi-layer MoS ₂ flake on which the experiments were performed and the SiO ₂ substrate on which the flake was deposited. (b) Large-scale friction force map recorded on an area that includes the single-layer region of the MoS ₂ flake and the SiO ₂ substrate, demonstrating the lubricating effect of MoS ₂ (bright: high friction; dark: low friction). The mean friction force recorded on MoS ₂ is ~ 2.5 times smaller than the one recorded on SiO ₂ . (c) Small-scale friction force map recorded on single-layer MoS ₂ , showing atomic-scale stick-slip.	15
2.2	Friction force as a function of the logarithm of the sliding speed (in units of nm/s) for single-layer (black circles) and bulk (red triangles) MoS ₂ samples, demonstrating very similar dependencies of friction force on sliding speed. The solid lines are fits by the PTT model.	16

2.3	Friction force as a function of the logarithm of the sliding speed (in units of nm/s) for three consecutive runs (Run 1: black squares, Run 2: red circles, and Run 3: blue triangles) performed on a particular area of the single-layer MoS ₂ sample, demonstrating increasingly stronger dependencies of friction force on sliding speed. The solid lines are fits by the PTT model.	19
3.1	(a) Friction map acquired on a multi-layer (2L: two layers, 3L: three layers, 4L: four layers) MoS ₂ flake, where brighter colors correspond to higher friction. While decreasing friction with increasing number of layers is observed (whereby, on average, 3L and 4L exhibit 71% and 50% of the friction recorded on 2L, respectively), no evidence of ripples can be detected. (b) Amplitude-modulation (i.e. tapping-mode) atomic force microscopy image of the topography associated with a multi-layer MoS ₂ flake on a SiO ₂ substrate (color scale range: 10 nm). No trace of linearly aligned ripples is found on the MoS ₂ flake. (c) Topography image recorded via frequency-modulation atomic force microscopy on a few-layer MoS ₂ flake, revealing the presence of linearly aligned, atomic-scale ripples on MoS ₂ , highlighted by black arrows (color scale range: 5 Å). The height of the highlighted ripples ranges from 1 Å to 3 Å.	23
3.2	(a) Schematic demonstrating the surface topography being imaged at varying tip-sample distances by changing the frequency shift (Δf_0) of the AFM. The oscillation amplitude of the cantilever is kept constant at 10 nm by employing an active feedback of excitation signal, <i>ad</i> . Three-dimensional topography and resonance frequency shift data are utilized to reconstruct tip-sample interaction potential. (b-f) Maps of tip-sample interaction energy at different tip-sample distances recorded over the same location as in Figure 3.1c. The average tip-sample interaction energy at each tip-sample distance was subtracted from the data to highlight corrugations. The color scale range decreases from 87 meV in (b) to 7 meV in (f). (g) Average tip-sample interaction energy as a function of tip-sample distance. The tip-sample distances and the average tip-sample interaction energies corresponding to the data presented in (b) to (f) are highlighted on the plot.	25
3.3	Friction anisotropy on MoS ₂ . (a) Ratios of friction forces recorded on SiO ₂ and MoS ₂ , as a function of rotation angle, extracted from a scan of 8 $\mu\text{m} \times 8 \mu\text{m}$ in size. Periodic behavior with nearly 2-fold symmetry is observed. (b) Friction force recorded on MoS ₂ as a function of rotation angle, extracted from a scan of 50 nm \times 50 nm in size. Periodic behavior with nearly 4-fold symmetry is observed. (c) Friction force recorded on MoS ₂ as a function of rotation angle, extracted from a scan of 1.5 $\mu\text{m} \times 1.5 \mu\text{m}$ in size, showing non-periodic character. . . .	27

3.4	Dependence of friction anisotropy on scan size. The relative probabilities of encountering a particular type of spatial symmetry (2-, 3-, 4-, 6-fold as well as no symmetry at all) on lateral force maps derived from the three-dimensional potential energy data presented in Figure 3.2, as a function of scan size (ranging from 256 nm ² to 62,500 nm ²). While 2-fold symmetry, due to the presence of ripples, dominates the probability distribution at large scan sizes, the “no symmetry” state is dominant for smaller scans. A non-negligible observation of 4-fold symmetry for large scan sizes can be potentially attributed to the presence of surface structures other than linearly aligned ripples.	28
3.5	A large-scale (1,000 nm × 1,000 nm) topographical image (in isometric, pseudo-3D form; color scale range: 4.2 nm) of the MoS ₂ flake acquired via high-resolution FM-AFM, including the region with linearly aligned ripples investigated in Figs. 3.1c and 3.2 (dashed white rectangle), a representative region where there are no discernible ripples (area highlighted with the blue dashed lines) and a ripple that changes direction by ~120° (dashed white lines), in accordance with the atomic symmetry of MoS ₂	29
3.6	A map (250 nm × 250 nm) of energy dissipation recorded simultaneously with the high-resolution topographical image of Figure 3.1c (color scale range: 1.8 meV). The lack of contrast demonstrates that the ripples observed in the topography map are indeed inherent structural features and not clusters formed by adsorbates from the environment.	30
4.1	Illustration of the formation of a "pucker" in front of an AFM probe tip sliding on single-layer graphene [43]. Similar mechanisms are believed to occur during the investigation of other 2D materials, including MoS ₂	33
4.2	(a) Friction force map of an undoped MoS ₂ flake with 1, 2, 3, 4, and 5 layers, situated on a SiO ₂ substrate. (b) Friction on MoS ₂ areas with different layer thicknesses. Friction is normalized to the value obtained on the 1L area.	34
4.3	(a) Friction force map obtained on a Re-doped MoS ₂ flake with 1, 2, and 3 layers, situated on a SiO ₂ substrate. (b) Friction on Re-doped MoS ₂ areas with different layer thicknesses. Friction is normalized to the value obtained on the 3L area.	35
4.4	Friction force values measured on 2, 11, 13, 14, and 15 layers of Re-doped MoS ₂ on a SiO ₂ substrate. Friction is normalized to the value obtained on the 14L sample (i.e. the maximum friction value).	35
4.5	Roughness values measured on 1-, 2-, 3-layer and bulk regions of (a) undoped MoS ₂ , and (b) Re-doped MoS ₂ extracted from 10 nm × 10 nm scans.	36

4.6	Adhesion force values measured on (a) 1-, 2-, 3-, 4-layer and bulk regions of undoped MoS ₂ , and (b) 1-, 2-, and 3-layer and bulk regions of Re-doped MoS ₂	37
-----	--	----

List of Tables

2.1	Parameters (F^* , β , and f_0) extracted from the fits of the data presented in Figure 2.2 via Eqs. (2.1) and (2.2) and experimentally obtained effective lateral stiffness values (k_{eff}) for measurements on single-layer and bulk MoS ₂	18
2.2	Parameters (F^* , β , and f_0) extracted from the fits of the data presented in Figure 2.3 via Eqs. (2.1) and (2.2) and experimentally obtained effective lateral stiffness values (k_{eff}) for three measurement runs on single-layer MoS ₂	20

Chapter 1

Introduction

1.1 Tribology: A Brief Summary

It is almost impossible to see a mechanical system which is not affected by friction and wear. Friction is sometimes helpful; for example, we can easily walk thanks to friction between our foot and the floor. However, friction can also decrease the efficiency of mechanical systems or even cause failure. Friction constitutes a tremendous issue in the modern world as we know that almost a quarter of the world's total energy output is used to overcome friction and is thereby lost [1]. A large number of equipment failures are also linked to friction and wear [2]. Whether we consider a complex, macroscale mechanical system such as a car engine or atomic-scale interactions between nanoscale objects, friction is a crucial phenomenon for all moving bodies.

The word, tribology, is derived from "tribos" which is a Greek word meaning "rubbing" and was coined for the first time in the 20th century. However, the empirical idea of tribology goes back into pre-historical times [3]. It is well known that people used two pieces of wood or rock to start a fire by simply rubbing them together for a certain amount of time [4]. They also used water, animal fat and mud as lubricants [5]. For example, in an old but famous Egyptian picture, slaves are pulling the gigantic grave of Tehuti-Hetep, in El-Bersheh. There is a man on the statue pouring a liquid lubricant, possibly some form of oil or water, to make transportation easier and faster for slaves by reducing the friction between the ground and the sled [5-7].

Leonardo da Vinci (1452–1519), who was both a successful military engineer and a great artist, is probably the first person in history who approached friction scientifically [5]. He studied friction for 10 years before painting his Renaissance masterwork "Mona Lisa" [8]. His experimental setup consisted of a rectangular block sliding over a flat surface. After his basic experiments, he came up with the idea of the coefficient of friction which is the ratio of the friction force and the normal force. His findings waited inside his notebook for hundreds of years since he did not publish them during his lifetime. Roughly 200 years later, in 1699, a French physicist known

as Guillaume Amontons studied dry sliding between two flat surfaces and introduced the concept of friction to the scientific community. He came up with 2 empirical yet important postulates, which are known as Amontons' Laws: First, the friction force is directly proportional to the normal force. This also implies that the coefficient of friction is independent of the normal load. Secondly, the friction force and the coefficient of friction are independent of the contact area between the two surfaces in relative motion [9]. These observations can be formulated as follows:

$$F_f = \mu N \tag{1.1}$$

where F_f is the friction force, μ is the coefficient of friction which is a material- and condition-specific constant and N is the normal load. Another French physicist, Charles-Augustin Coulomb reproduced these experimental results and verified Amontons' findings. Coulomb also came up with another empirical postulate; the friction force and the coefficient of friction are independent of the sliding speed once motion starts [6,7]. As shown by many studies throughout history, these three postulates are completely empirical and they do not work in many situations, not only on the nanoscale but also in the macroscopic world. Consequently, our understanding of friction is still evolving and the importance of the scientific approach in uncovering its fundamentals is well understood.

1.2 Nanotribology

The invention of the surface force apparatus (SFA), which is a scientific instrumental technique pioneered in 1969 by Tabor and Winterton [10], jumpstarted the field of "nanotribology", by allowing the measurement of interaction forces between two surfaces at miniscule length scales. In this technique, two surfaces are brought together and retracted in a very precise fashion. A beam interferometry system is used to record surface separation in detail and measure surface forces precisely. It is also possible to observe surface deformations and contact areas when two surfaces are brought together. Until the 20th century, tribologists were unaware of the fact that there is a huge difference between apparent area of contact and real area of contact [11]. For the surfaces brought into contact, the real area of contact, which is a function of the surface texture, material properties, and interface loading conditions, is hundreds to millions of times less than apparent contact area [12]. The real contact area can be considered as a sum of surface asperities of the two surfaces that are in contact (Figure 1.1). Obtaining precise information about the real contact area is a vital part of modern tribology research since it directly affects adhesion, friction and wear. The understanding of the true nature of real contact area has opened a new door and thus gave a start to modern nanotribology research, which rapidly accelerated with the introduction of the atomic force microscope (AFM) [13].

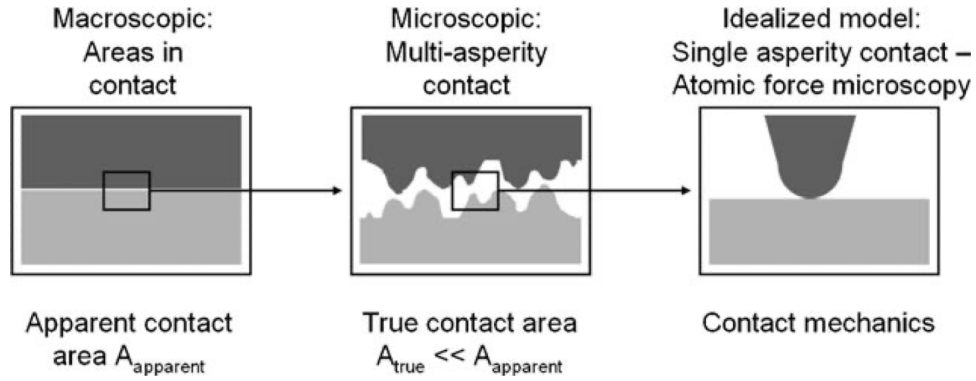


Figure 1.1: Evolution from an apparent contact area to idealized single asperity contact, such as that achieved by an AFM probe [14].

1.3 Atomic Force Microscopy

The invention of the Scanning Tunneling Microscope (STM) in 1981 by Gerd Binnig and Heinrich Rohrer at IBM Zurich, started the era of Scanning Probe Microscopy (SPM), which for the first time allowed scientists to visualize surfaces on atomic length scales, unlimited by the wavelength of light which severely constrained optical microscopy methods [15]. The invention of STM was rapidly followed by the rethinking of the method and the resulting invention of AFM by Binnig, Quate and Gerber in 1986 [13] (Figure 1.2).

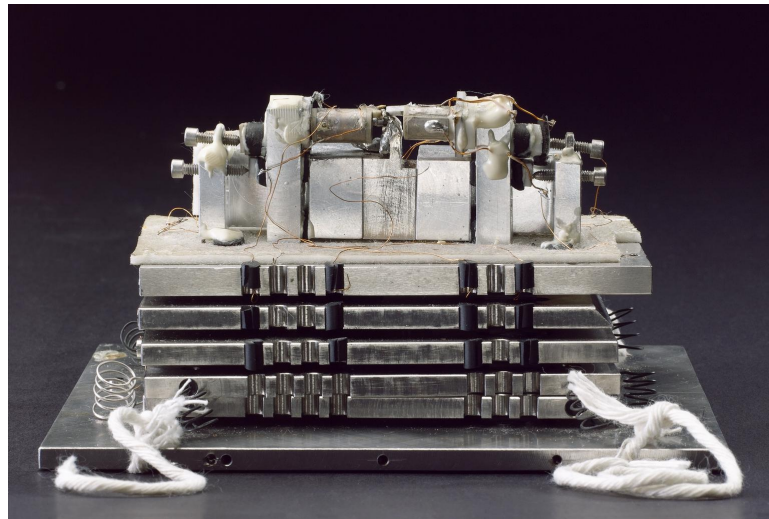


Figure 1.2: The first atomic force microscope invented by Gerd Binnig *et al.* at IBM Research Laboratory in Zurich [16].

Using the method of AFM, it is possible to directly measure tip-sample interactions in the form of forces that occur between a very sharp (radii of curvature on the scale of a few nanometers) tip and a sample surface of interest (which can

be electrically insulating, as opposed to STM). With AFM, it is possible to obtain ultra-high (sub-nm) resolution topographical maps of the scanned surface and at the same time measure forces smaller than a nN [17]. The capability of high-precision force detection is thanks to the fact that sharp AFM tips discussed above are attached to soft, micro-machined cantilevers with typical spring constants between 0.1 N/m and 1 N/m. Depending on the deflection sensitivity of the AFM instrument, forces on the order of pN can thus be measured using standard, commercial AFM probes. During a standard measurement performed in the contact mode, the sharp tip apex comes into contact with the surface in a controlled fashion thanks to a sensitive piezoelectric scanner (Figure 1.3). The desired area is scanned by *rasterization* at a given scanning rate using the piezoelectric scanner again. During these measurements, by way of a feedback loop, it is possible to keep interaction forces constant to keep contact with the surface and the sharp tip apex at a stable state. By recording the cantilever base position at each point of the scanned area with respect to its initial position, topographical surface maps are obtained. To measure the forces experienced at the tip-sample interface, a laser beam deflection method is used. A focused laser beam is directed on the back side of a cantilever. Using an adjustable mirror, the reflected beam is directed onto a four-quadrant photodetector. The vertical deflection of the cantilever is measured via a differential signal from the top and bottom quadrants. During scanning, the tip apex moves over the surface and this leads to momentary changes in cantilever deflection, and consequently the position of the laser beam on the photodetector. By following the differential signal from the top and bottom quadrants, and using a feedback loop to keep the signal at a constant level by changing the vertical position of the cantilever base, a surface topography map is generated. The lateral scanning size limit of a typical commercially available AFM is about $30\ \mu\text{m} \times 30\ \mu\text{m}$. While it is possible to change the number of pixels in a given AFM image, in most published research, AFM maps are standardized at 256 lines with 256 points each.

1.4 Lateral Force Microscopy

Using the method of Lateral Force Microscopy (LFM), it is possible to obtain maps of surface topography and lateral forces experienced by the AFM tip apex as it scans over the sample surface, at the same time. This has obvious implications for the study of frictional properties on the nanometer scale, essentially at a *single asperity*, thus overcoming a main limitation of tribological measurements at micro- and macroscopic length scales. While scanning the surface laterally, the very sharp tip apex experiences lateral forces caused by friction between the tip and the sample. These forces cause a torsional twisting of the cantilever. The torsional deformation of the cantilever leads to a horizontal change in the position of the directed laser beam on the four-quadrant photodetector. The differential signal from the left and right quadrants at each pixel of the scan thus gives information about the frictional forces experienced by the tip at a specific position on the sample. By gathering together

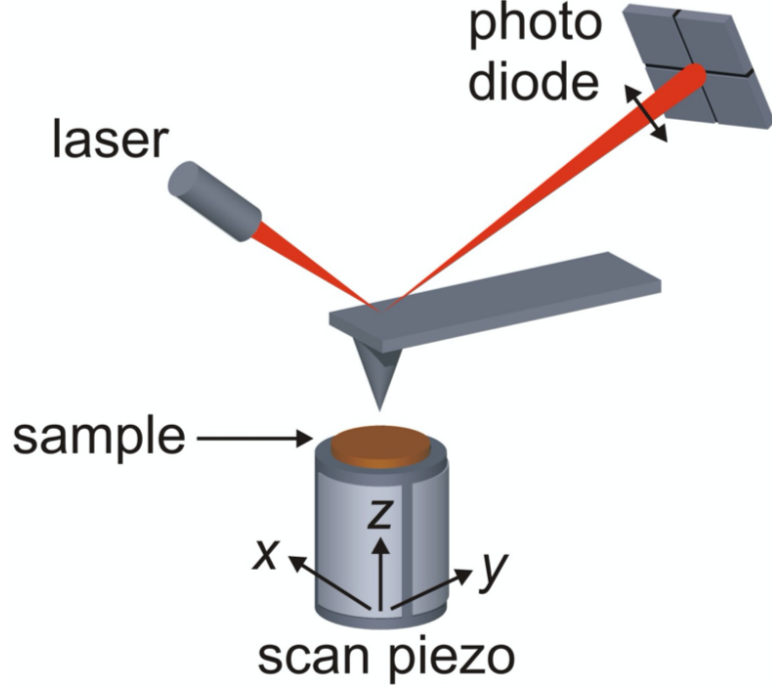


Figure 1.3: A basic representation of the AFM setup [18].

all data points, it is also possible to obtain lateral force / friction maps with high resolution and do research on the nano-scale aspects of the friction phenomenon. The normal and lateral movements of the focused laser beam on the four-quadrant photodetector are electrical signals. To convert these signals into forces, calibration needs to be performed (see Section 1.5). The normal (F_n) and lateral forces (F_l) between the tip and sample can be formulated as:

$$F_n = \theta_z((A + B) - (C + D)) \quad (1.2)$$

$$F_l = \alpha((A + C) - (B + D)) \quad (1.3)$$

where θ_z is the force calibration coefficient in the vertical z-direction, calculated simply by the product of the specific spring constant of the cantilever during the scan and the photo-detector sensitivity in nm/V, α is the lateral force calibration constant, and A, B, C, D are the electrical signals recorded by the four quadrants of the photodetector, in V (Figure 1.4).

To obtain nanoscale friction maps, lateral trace (i.e. forward scanning direction) and lateral retrace (i.e. backward scanning direction) maps are used [19]. Before starting a measurement, the laser position on the photodiode is adjusted to be in the center, i.e. origin. In this way, the starting values of normal and lateral forces are considered to be zero. When the scanning process is started, the lateral and vertical signals at each data point are calculated using that reference position.

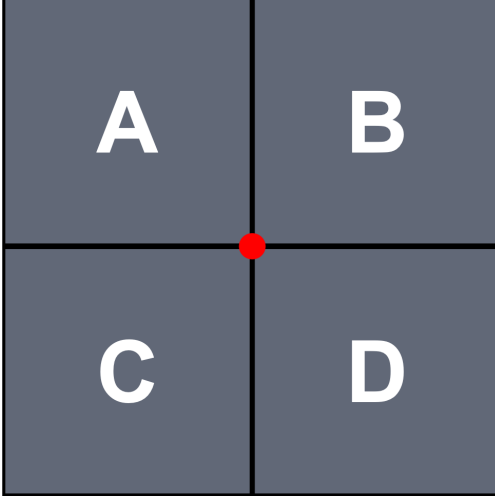


Figure 1.4: A sketch of the 4-quadrant photodetector with a red laser spot at the center.

However, during measurements, the zero reference point is likely to change and shift away from zero due to thermal drift and other effects. To overcome this undesired shift, friction force experienced by the tip is calculated by following the half-width (W) of the loop formed by lateral forces in the forward and backward directions (Figure 1.5) [19].

$$W = \frac{F_{l,forward} - F_{l,backward}}{2} \quad (1.4)$$

where $F_{l,forward}$ and $F_{l,backward}$ are the lateral forces in the forward and backward scan directions.

The offset (D) can also be calculated using the lateral forces in the forward and backward directions and it gives information on how the laser position on the photodiode has shifted from the initially determined zero position as follows:

$$D = \frac{F_{l,forward} + F_{l,backward}}{2} \quad (1.5)$$

It is important to note that lateral forces in the forward and backward direction have opposite signs. The very simple reason for this fact is while scanning in the forward direction, the cantilever is twisted clockwise (counter-clockwise). However, when the cantilever changes its scan direction, it is twisted in the counter-clockwise (clockwise) direction by experiencing lateral forces in the opposing direction. This continuously changes the reflected laser position on the photodiode between right and left, which results in positive and negative readings. The illustration in Figure 1.5 demonstrates the recording of the lateral force signal in a single scan cycle in the forward and backward directions in the LFM mode.

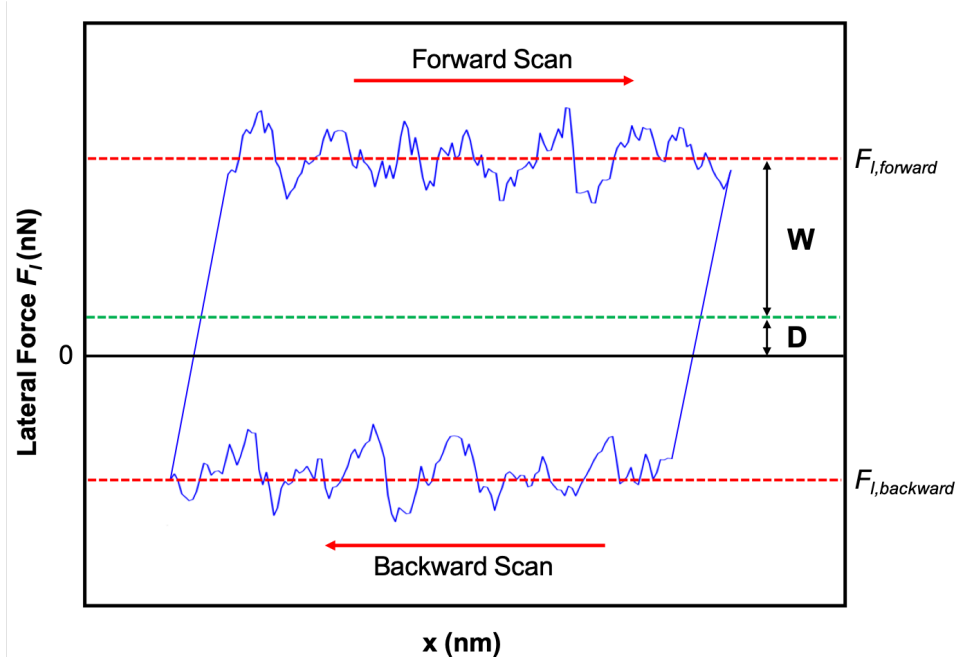


Figure 1.5: Schematic illustration of a friction loop, showing the forward and backward lateral force signals over one scan line, the half-width of the loop (W), and the offset value from zero (D).

1.5 AFM Tip Calibration

To perform AFM measurements, commercial micromachined cantilevers are typically utilized. There are a large number of cantilevers on the market depending on the operation mode and the physical properties of the surface to be studied. Each type of cantilever may have different stiffness, resonance frequency, radius of curvature, length, width, thickness, tip geometry, and coating material. These characteristics affect the measurements directly and dramatically. To convert electrical signals coming from the four-quadrant photodetector into physically meaningful force (normal and lateral) values, calibration for each AFM probe needs to be performed. We report here two methods that we employ to calibrate AFM probes for normal and lateral force measurements.

1.5.1 Normal Calibration

A standard calibration method for the determination of the normal cantilever stiffness (k), referred to as the Sader method [20,21], is used in this work. In the Sader method, the geometric properties of the cantilever probe and its resonance frequency are used to determine k using the following formula:

$$k = M_e b h L \rho_c w_{vac}^2 \quad (1.6)$$

where k is the stiffness of the cantilever, M_e is the effective mass of the cantilever, b , h , and L are the width, length, and thickness of the cantilever, respectively, ρ_c is the density of the cantilever material, and w_{vac} is the angular resonance frequency of the cantilever in vacuum. The cantilevers used for the experiments reported in the following chapters have been calibrated using the Sader method, and k values range from 0.05 N/m to 0.9 N/m. AFM cantilevers with stiffness values below 1 N/m are generally considered to be "soft". If the stiffness is above 40 N/m, they are referred to as "stiff" cantilevers. After determining cantilever stiffness, the calculation of the force is very simple using Hooke's law:

$$F = kz \tag{1.7}$$

where z is the vertical deflection of the cantilever at a given location and F is the force in the normal (i.e. vertical) direction.

1.5.2 Lateral Calibration

The lateral calibration of the AFM cantilever is a bit more complex than its normal calibration. Again, there are various methods such as the lever method, axial sliding method, torsional added mass method, and wedge method to calibrate cantilevers in the lateral direction [22]. The cantilevers used in the experiments reported in this thesis are calibrated using an improved wedge calibration method proposed by Varenberg et al. [23], using the MikroMasch TGF 11 silicon calibration grating with well-defined wedges and wedge angles (Figure 1.6). During lateral calibration, the calibration grating is scanned with a constant speed along the wedges in forward and backward direction to obtain lateral deflection maps. Each time, the applied force during the measurements is increased while keeping the scanning speed constant on the same area of scan, i.e. one can record 10 different maps of the same area with 0.5 nN increments in normal force to obtain a reasonable data set. In this way, friction loops are obtained for each applied load corresponding to a different scan. In the next step, friction loop half-width (W) and friction loop offset (D) for each applied load are determined. Using the following equations, the lateral force calibration constant α with units of N/V, and the friction coefficient μ are calculated [24]:

$$\alpha W_0 = \frac{\mu}{\cos^2\theta - \mu^2 \sin^2\theta} \tag{1.8}$$

$$\alpha D_0 = \frac{(1 + \mu^2) \sin\theta \cos\theta}{\cos^2\theta - \mu^2 \sin^2\theta} \tag{1.9}$$

where θ is the angle of the wedges, which is $54^\circ 44'$ for the MikroMasch TGF 11 silicon calibration grating, and D_0 and W_0 are the slopes of D and W with respect to applied load. This calculation can be done for both the upward and downward slope of a given wedge, and the average of these calculations can be used to increase statistical significance. After calculating α with units of N/V, it is possible to convert

the lateral force signal readings from the AFM in units of V to physically meaningful units of N by simply multiplying them with α (Eq. 1.3).

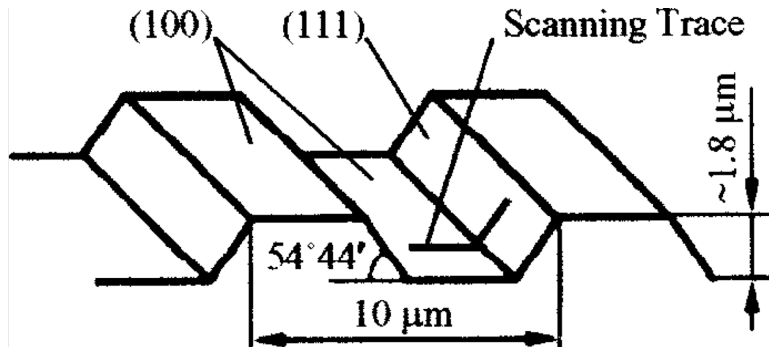


Figure 1.6: Schematic representation of the MikroMasch TGF 11 silicon calibration grating with well-defined wedges used in the lateral calibration of all cantilevers utilized in this work [23].

1.6 Force Spectroscopy

When two bodies are brought into contact, adhesive forces are observed due to interatomic interactions between the surfaces of the bodies in the form of chemical and physical forces. Using an AFM, it is possible to precisely measure these forces between a sharp probe apex and a sample surface by recording force vs. distance curves, i.e. by performing force spectroscopy [25] (Figure 1.7). In this mode, the cantilever probe starts sufficiently away from the surface such that interactions are negligible and then approaches the surface while the cantilever deflection (directly correlated with tip-sample interaction forces) is detected. At a particular distance, the cantilever is suddenly “pulled in” by the sample due to attractive (i.e. negative) interactions and a sharp drop in the force reading is observed. Then, the cantilever keeps pushing on the surface and the force signal (now repulsive, i.e. positive) starts to increase while the cantilever bends until a force limit is reached. At this position, the withdrawal of the cantilever is initiated. The force signal starts to decrease until the snap-off point when the cantilevers “jumps” back from the surface to its equilibrium point. The magnitude of the change in the force from the snap-off point to the equilibrium position thus equals the adhesion force, while the slope of the force-distance curve in the repulsive interaction regime is related to the stiffness of the sample.

1.7 MoS₂: Physical and Lubricative Properties

Two-dimensional (2D) materials have attracted tremendous research interest following the mechanical exfoliation of single-layer graphene from its three-dimensional (3D) bulk form, graphite in 2004 [26]. In other words, the

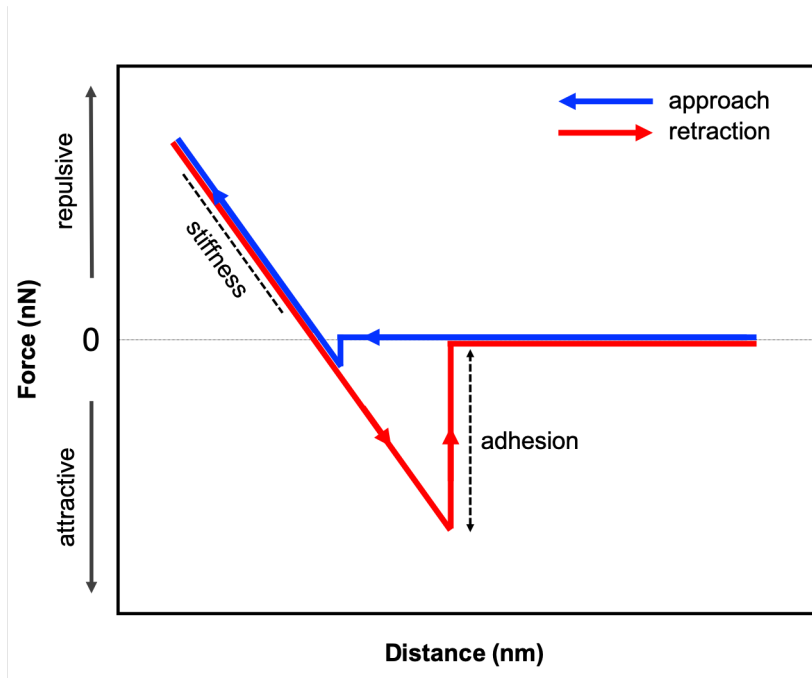


Figure 1.7: Schematic representation of a typical force vs. distance curve.

discovery that atomically thin sheets can be isolated from bulk crystals and the exciting physical properties exhibited by them, initiated the thriving field of 2D materials. Over a span of more than 15 years, the electrical, mechanical, and chemical properties of 2D materials – including graphene, molybdenum disulfide (MoS_2) and others – were studied in great detail [27-30], revealing extraordinary characteristics that could eventually allow revolutionary applications in diverse areas of science and technology.

Transition metal dichalcogenides (TMDCs) are an important class of 2D materials [31]. One of the most studied and prominent members of TMDCs is molybdenum disulfide (MoS_2). Monolayer MoS_2 is a semiconductor with a direct bandgap of 1.8 eV along with carrier mobility of $200 \text{ cm}^2/\text{Vs}$ [32], which has a great advantage over gapless graphene for many applications including but not limited to micro-/nano- electromechanical systems. Molybdenite is widely available in nature, and to synthesize MoS_2 , exfoliation and CVD synthesis methods are commonly used in research laboratories. Monolayer MoS_2 consists of Mo (+4) and S (-2) atoms in a way such that covalent bonds in the order of S-Mo-S are formed [33] (Figure 1.8). The thickness of a single layer MoS_2 is 3.25 \AA . In the bulk form of the material, these individual layers are connected by weak van der Waals forces with an interlayer spacing of 6.15 \AA . MoS_2 is classified as mechanically flexible with Young's modulus of $0.33 \pm 0.07 \text{ TPa}$ [34]. Its shear strength under normal load is measured as 24.6 MPa [35], thus, its superlubric properties are also under investigation. The in-plane stiffness of single-layer MoS_2 is $\sim 270 \pm 100 \text{ GPa}$ while the average breaking strength is $\sim 23 \text{ GPa}$ [36].

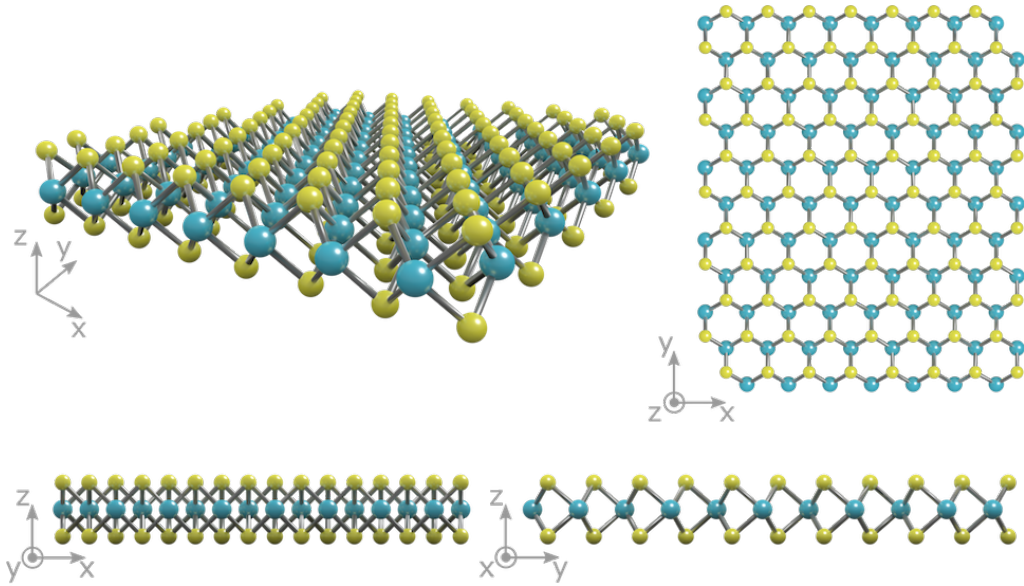


Figure 1.8: The crystal structure of monolayer MoS_2 in different views. Mo is shown in turquoise and S in yellow [39].

While the majority of work in the literature has centered on their unusual electronic properties and the related implications for devices, the mechanical characteristics of 2D materials, such as their elastic deformation [37] and failure mechanisms [38] are also of immense interest [30]. Another area of inquiry in terms of mechanical properties of 2D materials involves their tribology. Specifically, the potential use of 2D materials as solid lubricants in micro- and nano-scale mechanical systems draws significant attention, mainly due to the fact that liquid-based lubrication schemes are not easily applicable on such small length scales [40-42]. Consequently, friction on 2D materials was evaluated in a number of studies conducted primarily via AFM, focusing on the effects of applied load, number of layers, structural defects and humidity, among others [43-50].

MoS_2 , in particular, is widely used as a solid lubricant in bulk form or employed as an additive in liquid lubricants. The bulk form of MoS_2 is the most commonly used solid lubricant for space and high-altitude applications. As opposed to graphite, the lubricative properties of MoS_2 do not degrade in vacuum conditions but improve [51]. It preserves its lubricative properties from the cryogenic temperatures to several hundred degrees Celsius [52]. Hence, along with the other advantages, MoS_2 is considered as a novel lubricant for the aerospace/space industry especially for space vehicles and robots working under the extreme conditions of outer space.

Motivated as above, we have attempted in this thesis to contribute to the formation of a comprehensive understanding of the nanotribology of MoS_2 , by focusing on a few key pieces of missing information in the literature. In particular, we have characterized the speed dependence of friction on MoS_2 , tried to understand

the underlying reasons for its friction anisotropy and ultimately discovered an unusual layer-dependence of friction on Re-doped MoS₂ samples.

1.8 Outline

The following parts of this thesis consist of four chapters:

In Chapter 2, friction forces are investigated as a function of sliding speed on mechanically exfoliated, single-layer and bulk molybdenum disulfide (MoS₂). The results of the experiments are discussed in detail by taking into account (i) the number of layers of MoS₂, and (ii) the physical characteristics of the AFM probe.

In Chapter 3, a detailed discussion of friction anisotropy, caused by atomic-scale ripples on MoS₂, is presented. LFM results are complemented by three-dimensional force/energy spectroscopy measurements performed using frequency modulation atomic force microscopy (FM-AFM), in collaboration with Dr. Omur E. Dagdeviren at McGill University.

In Chapter 4, the nanotribological properties of mechanically-exfoliated, Re-doped MoS₂ are discussed and compared with undoped MoS₂, whereby an anomalous, inverse layer-dependence trend is observed.

Lastly, in Chapter 5, a brief summary of the thesis is presented with an outlook regarding future directions of nanotribology research on MoS₂.

Chapter 2

Speed Dependence of Friction on MoS₂

2.1 Speed Dependence of Friction

Despite the extensive amount of work performed toward elucidating friction mechanisms on 2D materials, very few results were published on the dependence of friction forces on sliding speed [53]. This is potentially a critical concern, as components in various micro- and nano-scale mechanical systems designed to be lubricated by 2D materials are expected to move in a wide range of speeds during operation. As such, a potential degradation of lubricative character at certain sliding speeds could result in unexpected device failure and consequently necessitate new approaches in component design.

Aside from the practical concerns described above, the general question of whether or how friction depends on sliding speed is a subject of ongoing research. Coulomb's experiments, performed in the 18th century, have led to the conclusion that friction does not depend on sliding speed, which is considered to be one of the "classical" laws of friction [7]. On the other hand, the use of AFM in friction research revealed a variety of speed dependencies for friction on the nanoscale, with certain studies pointing to a logarithmic increase of friction with sliding speed [54-57], while others have found no dependence [58] and even decreasing friction with increasing speed based on variations in interface chemistry [59] or normal load [60].

In this part of the thesis, we utilize AFM to investigate the speed dependence of friction on mechanically exfoliated, single-layer and bulk samples of MoS₂. The motivation to focus on MoS₂ stems partially from the fact that, in its bulk form, it is widely employed as a solid lubricant, either by itself or as an additive in liquid lubricants [61]. As indicated before, the lubricative properties of MoS₂ improve significantly under vacuum (as opposed to graphite, the bulk form of graphene), making it an attractive solid lubricant for applications including but not limited to spacecraft components [62]. Consequently, single- and few-layer MoS₂ have the

potential to be an effective solid lubricant for micro- and nano-scale mechanical systems designed for operation under low humidity or vacuum conditions.

2.2 Methods and Materials

The experiments reported in this chapter were performed under ordinary laboratory conditions using a commercial AFM instrument (Asylum Research, Cypher VRS). MoS₂ flakes were prepared by mechanical exfoliation of a bulk MoS₂ crystal onto SiO₂ substrates [26]. The measurements were conducted using two types of silicon cantilevers (MikroMasch HQ:CSC38 and Bruker RESPA-20), with normal spring constant values (0.05 N/m and 0.36 N/m, respectively) determined by the Sader method [21] discussed in Section 1.5.1. The cantilevers were calibrated for lateral force measurements using the method introduced in Section 1.5.2. During the measurements, no normal load was applied to the cantilevers; as such, the effective normal load was solely due to adhesion. AFM measurements were performed in contact mode, whereby the lateral force signal was collected together with topography maps. The measurements focused on areas of a few nanometer-square on single-layer and bulk regions of a single MoS₂ flake, at scanning speeds ranging from 2.9 nm/s to 1560 nm/s. All lateral force maps collected in these experiments showed atomic-scale stick-slip character. In order to minimize the potential effect of gradual tip changes with varying time on the acquired data, the scanning speed was varied randomly [56]. The mean friction force corresponding to a particular measurement was determined from friction loops constructed from the forward and backward lateral force maps [19]. Four consecutive scans were performed at each scanning speed to increase statistical significance; the friction force reported for each speed (F_L) reflects the mean and standard deviation of these four measurements. The effective lateral stiffness at the tip-sample junction (k_{eff}) was experimentally determined from lateral force maps, by studying the slopes during the "stick" phase [54]. No significant change in k_{eff} values was observed with respect to scanning speed, in accordance with previous results [53].

Figure 2.1a shows a three-dimensional representation of a topographical AFM image which comprises the multi-layer MoS₂ flake on which the experiments were performed, as well as the SiO₂ substrate on which the flake was deposited. The shallowest part of the flake is about 1.0 nm higher than the underlying SiO₂ substrate; the highest part of the flake is at a height of ~ 20 nm and can thus be considered "bulk". Despite the fact that the value of ~ 1.0 nm is somewhat larger than what was reported for single-layer MoS₂ flakes in some studies (~ 0.8 nm) [63], the fact that it is significantly less than the minimum height for bi-layer MoS₂ (~ 1.3 nm) establishes that this region of the flake is indeed single-layer. While the large-scale friction force map in Figure 2.1b demonstrates the remarkable solid lubrication effect that is achieved on SiO₂ by single-layer MoS₂, the friction force map in Figure 2.1c exemplifies the atomic-scale stick-slip character that is observed in smaller scans, from which the speed dependence data presented in the following parts of this chapter have been extracted.

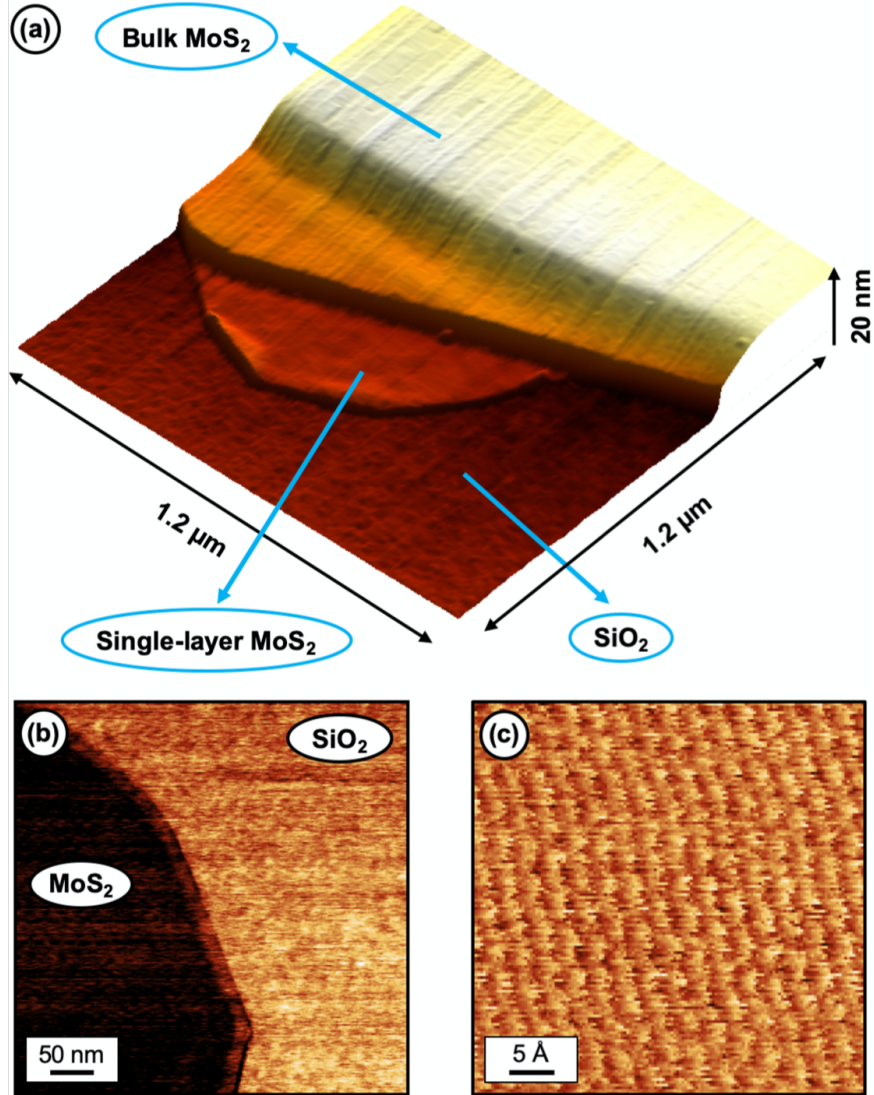


Figure 2.1: (a) Three-dimensional representation of a topographical AFM image showing the multi-layer MoS₂ flake on which the experiments were performed and the SiO₂ substrate on which the flake was deposited. (b) Large-scale friction force map recorded on an area that includes the single-layer region of the MoS₂ flake and the SiO₂ substrate, demonstrating the lubricating effect of MoS₂ (bright: high friction; dark: low friction). The mean friction force recorded on MoS₂ is ~ 2.5 times smaller than the one recorded on SiO₂. (c) Small-scale friction force map recorded on single-layer MoS₂, showing atomic-scale stick-slip.

2.3 Effect of Thickness

Figure 2.2 shows the friction force that was recorded as a function of scanning speed, by means of consecutive measurements on single-layer and bulk MoS₂ samples performed with the same cantilever (RESPA-20), over the course of a single day.

The results demonstrate that friction force increases logarithmically with sliding speed on both types of samples. Remarkably, the dependence of the experimentally acquired friction data on speed is very similar for both single-layer and bulk MoS₂, in contrast to results published recently for graphene. The logarithmic increase of friction with sliding speed can be understood by means of the thermally-activated Prandtl-Tomlinson (PTT) model [55,64].

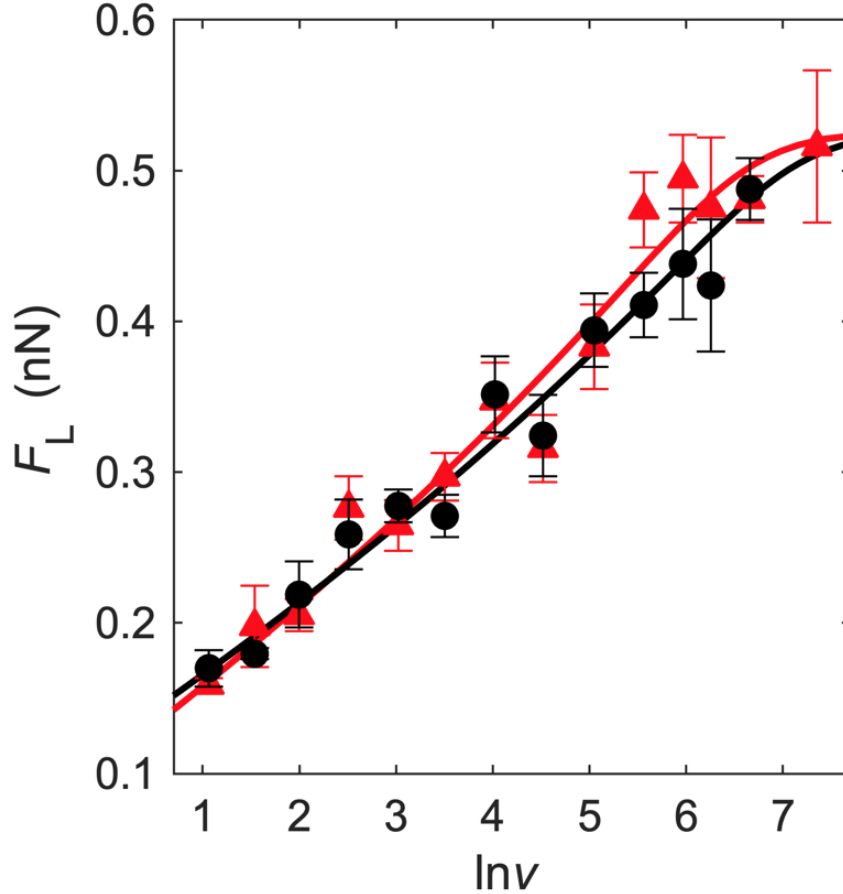


Figure 2.2: Friction force as a function of the logarithm of the sliding speed (in units of nm/s) for single-layer (black circles) and bulk (red triangles) MoS₂ samples, demonstrating very similar dependencies of friction force on sliding speed. The solid lines are fits by the PTT model.

In the classic Prandtl-Tomlinson model [65,66], a point mass (that represents the tip apex in AFM) is attached to a base (that represents the cantilever's fixed base in AFM) by means of an elastic spring (which represents the effective lateral stiffness of the sample-tip-cantilever system), whereby the base and consequently, the point mass, are moved laterally over a one-dimensional, periodic potential energy landscape that arises due to energy interactions between the tip apex and the sample surface. During this motion, the tip apex periodically gets stuck in the minima of the energy landscape. Due to fact that the base keeps moving with constant

speed over the sample surface, the model spring that connects the tip apex to the cantilever gets stretched with passing time, until the elastic energy stored in the spring is sufficient to overcome the potential energy barrier around the well, at which point the tip apex slips to the next potential minimum, with the energy stored in the spring being dissipated through phononic mechanisms. The repeated process of being stuck in and then slipping out of potential energy wells gives rise to the atomic-scale stick-slip character of lateral force maps such as the one shown in Figure 2.1c. The F_L recorded in the AFM experiments simply reflects the force experienced by the spring in the Prandtl-Tomlinson model. This relatively simple picture becomes slightly more complex when the effect of a non-zero temperature is considered. At a given temperature, the thermal energy associated with the tip apex facilitates its ability to slip to adjacent potential minima in the direction of motion, by effectively lowering the associated energy barrier. This also allows the formation of a basic understanding of the effect of sliding speed on friction: With increasing sliding speed, the number of attempts for thermally activated jumps in a given potential well decreases. This leads to a monotonic increase in F_L until a limiting value (i.e. a plateau) is reached at high speeds, representing the scenario when the base is moving so fast that thermally activated jumps can no longer lower the friction. Analytically, the overall picture is captured by the following equation [55]:

$$\frac{1}{\beta k_B T} (F^* - F_L)^{3/2} = \ln\left(\frac{v_0}{v}\right) - \frac{1}{2} \ln\left(1 - \frac{F_L}{F^*}\right) \quad (2.1)$$

where β is a parameter that depends on the shape of the tip-sample interaction potential, k_B is the Boltzmann constant, F^* is the "limiting value" of the friction force expected at temperature $T=0$ K or at sufficiently high sliding speeds, v is the sliding speed, and v_0 is a characteristic speed that depends on parameters β , F^* , k_{eff} , as well as the "attempt frequency" of the tip apex relevant for jumps to adjacent potential minima (f_0), in the following fashion:

$$v_0 = \frac{2f_0\beta k_B T}{3k_{eff}\sqrt{F^*}} \quad (2.2)$$

In order to analyze the speed dependence results presented in Figure 2.2 for single-layer and bulk MoS₂ in more detail, Eqs. 2.1 and 2.2 were utilized to fit the experimental data (solid lines in Figure 2.2), with F^* , β , and f_0 as free parameters. The obtained results for the parameters are reported in Table 2.1, where the experimentally recorded values for k_{eff} are also listed. As one can already see in Figure 2.2, the fits performed according to Eqs. 2.1 and 2.2 closely follow the experimental data, with very similar rates of increase of friction with sliding speed. This qualitative observation is reproduced by the similarity in obtained fit parameters, in particular by β and F^* . The close similarity in the obtained results suggests that the number of layers has no discernible effect on how friction depends on sliding speed for MoS₂, meaning that the key characteristics of the tip-sample interaction potential (embodied by β and F^*) do not significantly change with increasing number of MoS₂

layers. On the other hand, it needs to be considered that the specifics of the tip-sample interaction depend also on the atomic-scale physical characteristics of the tip apex itself. In particular, changes in the atomic structure of the tip apex can change the specifics of the interaction potential, e.g. by changing the depth of potential minima and/or the overall shape of the potential profile. Consequently, the similar results obtained for β and F^* on single-layer and bulk MoS₂ suggest that the atomic-scale characteristics of the tip apex were very similar for both sets of experiments, i.e. that there was no substantial tip change during the course of the measurements. This idea is further corroborated by observing that the k_{eff} values are nearly identical for both single-layer and bulk MoS₂. Finally, this latter finding implies that the in-plane stiffness of a MoS₂ layer (which plays a major role in determining k_{eff}) does not depend on the existence or absence of additional layers under it, which can be understood by considering the weak, van der Waals nature of the interaction between individual MoS₂ layers.

	F^* (nN)	$\beta(\times 10^6)(N^{3/2}/J)$	f_0 (kHz)	k_{eff} (N/m)
Single-Layer	0.53 ± 0.01	0.34 ± 0.02	13.9 ± 2.5	2.01 ± 0.79
Bulk	0.53 ± 0.01	0.39 ± 0.03	7.8 ± 1.5	2.02 ± 0.80

Table 2.1: Parameters (F^* , β , and f_0) extracted from the fits of the data presented in Figure 2.2 via Eqs. (2.1) and (2.2) and experimentally obtained effective lateral stiffness values (k_{eff}) for measurements on single-layer and bulk MoS₂.

2.4 Effect of AFM Probe Characteristics

To complement the results reported above, additional experiments were performed on single-layer MoS₂. In particular, friction on a particular area on the single-layer region was repeatedly measured as a function of sliding speed, in the form of three separate experimental runs performed over the course of two days with the same cantilever (HQ:CSC38). The results of the experiments, reported in Figure 2.3, are in striking contrast to Figure 2.2: The speed dependence of friction is significantly different for the three runs, with a clear increase in the rate with which friction increases with sliding speed. This observation is quantitatively captured by the fit parameters β and F^* that are reported in Table 2.2. In particular, β and F^* values significantly increase with each experimental run, to nearly four and three times their original values, respectively. Considering that all runs were performed on the same area of the same single-layer MoS₂ flake, the reported results lead to the conclusion that atomic-scale changes in the tip apex must have led to the observed differences in the speed dependence of friction. In particular, the increase in F^* could imply the formation of a larger (i.e. blunter) tip apex over time, resulting in a larger total friction force [56]. A study of the experimentally obtained lateral stiffness values at the tip-sample junction (k_{eff}) corroborates this conclusion: With

increasing number of runs, the tip-sample junction becomes stiffer, pointing to atomic-scale changes in the tip apex that result in laterally stiffer structures. While it is conceivable that this trend could saturate in a stable tip structure after a certain number of runs, substantial tip changes that frequently lead to a loss of atomic-scale stick-slip prevented such a study from being conducted.

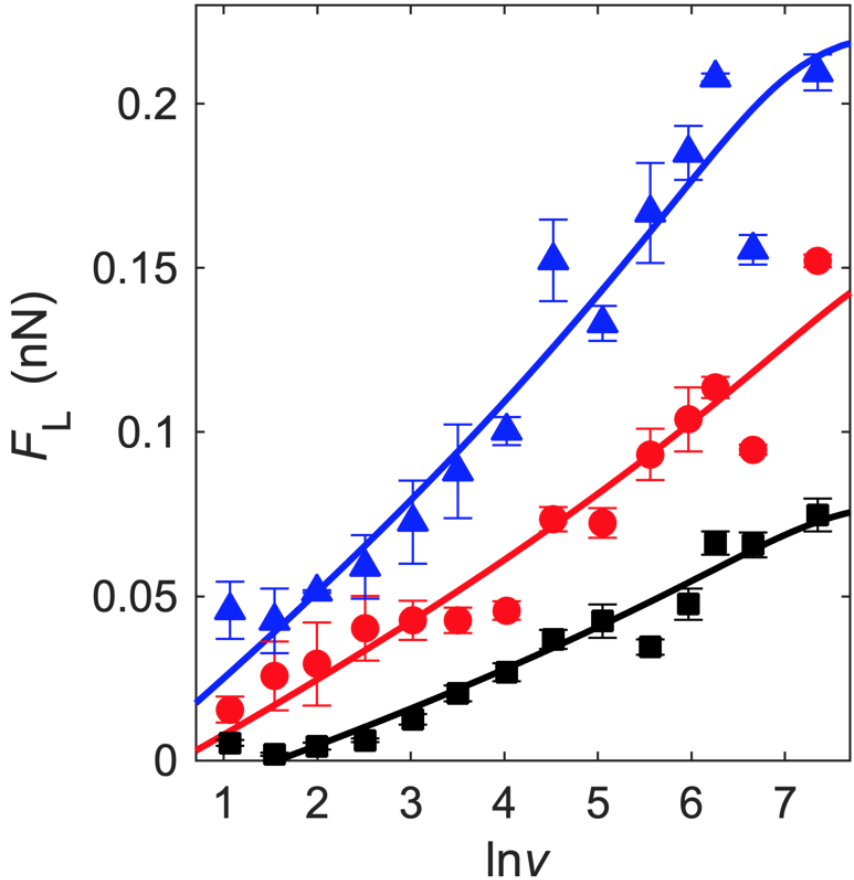


Figure 2.3: Friction force as a function of the logarithm of the sliding speed (in units of nm/s) for three consecutive runs (Run 1: black squares, Run 2: red circles, and Run 3: blue triangles) performed on a particular area of the single-layer MoS₂ sample, demonstrating increasingly stronger dependencies of friction force on sliding speed. The solid lines are fits by the PTT model.

A particular aspect of the analysis that has so far not been discussed is the fact that the obtained values for the attempt frequency f_0 reported in Tables 2.1 and 2.2 do not necessarily follow the trends observed for the other, tip-sample-interaction-specific parameters β , F^* , and k_{eff} . While f_0 values in our study are on the same order of magnitude as those reported in certain prior studies [55], it was also shown that f_0 is sensitive to the extent of the instrumental noise present during the measurements and how well it couples to the tip-sample junction [56,67]. As such, the differences in f_0 in our measurements can be potentially ascribed to changes in instrumental

	F^* (nN)	$\beta(\times 10^6)(N^{3/2}/J)$	f_0 (kHz)	k_{eff} (N/m)
Run I	0.079 ± 0.002	0.037 ± 0.003	20.2 ± 5.3	0.45 ± 0.10
Run II	0.160 ± 0.002	0.078 ± 0.007	28.9 ± 9.6	0.52 ± 0.09
Run III	0.223 ± 0.002	0.139 ± 0.014	7.2 ± 2.0	0.58 ± 0.08

Table 2.2: Parameters (F^* , β , and f_0) extracted from the fits of the data presented in Figure 2.3 via Eqs. (2.1) and (2.2) and experimentally obtained effective lateral stiffness values (k_{eff}) for three measurement runs on single-layer MoS₂.

noise. Finally, it needs to be mentioned that the lack of a plateau region in our experiments (with the potential exception of the bulk measurement in Figure 2.2 and Run 3 in Figure 2.3) prevents an independent verification of the fit parameter F^* , with the implication that there can be other combinations of parameters that could fit the experiments similarly well. This, however, does not change the main conclusions drawn earlier: (i) the rate with which friction increases with sliding speed on MoS₂ does not seem to depend on the number of layers and (ii) tip apex changes can significantly affect the speed dependence of friction on MoS₂.

In this chapter, we studied the speed dependence of friction on single-layer and bulk MoS₂ by means of atomic-scale, stick-slip lateral force maps acquired via AFM. Our results revealed a logarithmic dependence of friction on sliding speed, in accordance with the PTT model. It was found that the number of layers has no discernible effect on how friction scales with speed on MoS₂. Moreover, changes in the atomic structure of the tip apex manifesting in the form of variations in tip-sample-interaction-specific parameters of the PTT model as well as the effective lateral stiffness at the tip-sample junction were found to significantly affect the speed dependence of friction. The approach employed here can be extended to other 2D materials, where utmost care has to be exercised to analyze and if possible, exclude the effect of tip apex changes on the acquired data. The results reported in this chapter have been published in the form of a journal article [68].

Chapter 3

Imaging, Spectroscopy, and Friction Anisotropy of Atomic-scale Ripples on MoS₂

3.1 Atomic-scale Ripples on 2D Materials and Friction Anisotropy

Despite the prevalent scientific interest in 2D materials today, their very existence initially puzzled scientists, based on the idea that a perfectly two-dimensional crystalline sheet of material would be thermodynamically unstable [69]. Subsequent work revealed that such 2D materials may in fact exist in the presence of out-of-plane deformations with atomic-scale (< 1 nm) corrugations, also termed ripples [70,71]. The presence of ripples was confirmed by transmission electron microscopy (TEM) imaging performed on suspended single-layer graphene [70], as well as single-layer MoS₂ [72], although in an indirect fashion, i.e. by studying the broadening of diffraction spots in reciprocal space. Eventually, TEM experiments also allowed the direct visualization of atomic-scale ripples in suspended few-layer (up to ~ 10 layers) graphene samples in real space, with out-of-plane corrugations and lateral spacings on the order of 5 \AA and 500 \AA , respectively, largely in accordance with theoretical expectations [73]. Perhaps more importantly from an application point of view, scanning tunneling microscopy (STM) experiments demonstrated that the rippling of graphene is preserved even for samples that are supported on substrates such as silicon dioxide (SiO₂) [74], in an intrinsic fashion that is not related to the topographical features of the substrate itself.

Most prior work related to ripples focused on their effect on the electrical properties of 2D materials. For instance, the presence of ripples was found to suppress weak localization in graphene [75] and attempts were made to control the structure and distribution of ripples in order to tune electrical properties [76,77]. On the other hand, the number of studies focusing on the effect of ripples on the mechanical characteristics of 2D materials is much lower. A particular mechanical

phenomenon that was studied in detail on 2D materials is friction, based on the discovery that single- or few-layers of graphene, MoS₂ and other 2D materials function as effective solid lubricants on the nanoscale, where lubrication with fluids is impractical due to size effects [43]. The pioneering work on 2D material friction conducted via atomic force microscopy (AFM) [43] was soon followed by other AFM experiments on graphene that demonstrated a strong dependency of friction forces on the scanning direction, i.e. *friction anisotropy* [78]. A peculiar aspect of these milestone experiments was that the friction forces exhibited a 2-fold symmetry, in obvious contradiction to the 6-fold symmetry of the atomic structure of graphene. This observation, also made by other groups on other 2D materials including MoS₂ [79], was explained by the presumed existence of linearly aligned structures (i.e. ripples) on the material surface, leading to high (low) friction forces when the AFM tip is scanning across (along) the ripples on a particular region of the sample. Despite this seemingly widespread idea – together with a competing theory based on the presence of linearly aligned stripes formed by environmental adsorbates [80]–, the connection to friction anisotropy remains controversial, as the ripples are not directly observed during the experiments. Moreover, the literature also includes friction anisotropy studies that deviate from 2-fold symmetry [81,82].

In this chapter of the thesis, we first report results of a collaboration with McGill University that allow the imaging and interaction spectroscopy of atomic-scale ripples on few-layer, mechanically-exfoliated MoS₂ flakes. We then report results of friction anisotropy experiments on MoS₂, the explanation of which becomes possible by a detailed analysis of the interaction spectroscopy results.

3.2 Imaging of Atomic-scale Ripples on MoS₂

Motivated by the absence of AFM data in the literature demonstrating the presence of atomic-scale ripples on 2D materials, we performed experiments to answer the question of whether the imaging of atomic-scale ripples on MoS₂ can be accomplished with an AFM-based approach. Based on the defining role that ripples are thought to play in the friction anisotropy of such materials [78,79], we initially conducted LFM experiments on few-layer MoS₂ samples exfoliated onto SiO₂, whereby topographical and friction force maps are recorded simultaneously as the AFM tip slides on the sample surface in contact mode [12]. While the friction force map of Figure 3.1a, recorded on a multi-layer MoS₂ flake, clearly demonstrates the layer-dependence of friction that is a ubiquitous characteristic of 2D materials [43], no linearly aligned structures, i.e. ripples, are observed on the flake surface, along the lines of previous LFM work performed on this material [43,79,82].

Considering that LFM necessitates continuous contact between the AFM tip and the sample surface, which invariably results in the averaging of tip-sample interactions over a finite contact area and thus leads to a loss of spatial resolution [83], we directed our attention to alternative modes of AFM imaging. In particular, imaging via conventional tapping-mode AFM (performed by way of amplitude

modulation [84], with oscillation amplitudes on the order of 10 nm) did not result in the imaging of ripples either (Fig 3. 1b). This result is perhaps not surprising considering that tapping-mode AFM, despite the absence of a continuous contact between the tip and sample, still involves intermittent contact (manifesting in the form of repulsive tip-sample interactions), which also results in a loss of spatial resolution.

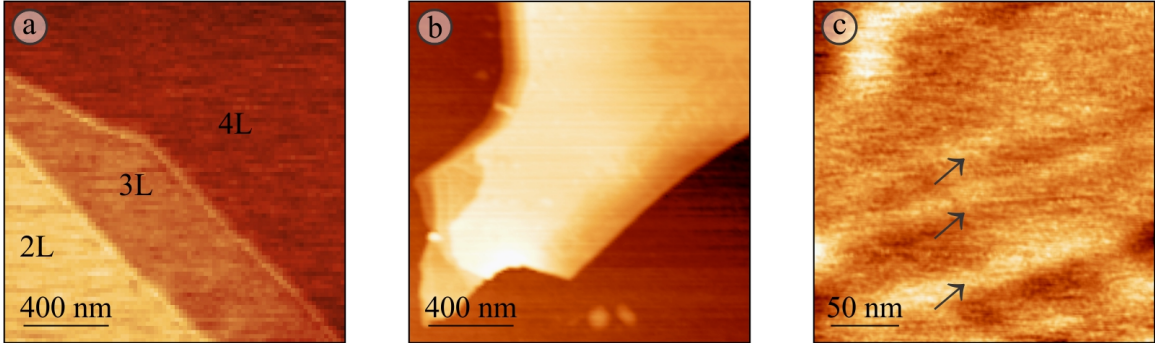


Figure 3.1: (a) Friction map acquired on a multi-layer (2L: two layers, 3L: three layers, 4L: four layers) MoS₂ flake, where brighter colors correspond to higher friction. While decreasing friction with increasing number of layers is observed (whereby, on average, 3L and 4L exhibit 71% and 50% of the friction recorded on 2L, respectively), no evidence of ripples can be detected. (b) Amplitude-modulation (i.e. tapping-mode) atomic force microscopy image of the topography associated with a multi-layer MoS₂ flake on a SiO₂ substrate (color scale range: 10 nm). No trace of linearly aligned ripples is found on the MoS₂ flake. (c) Topography image recorded via frequency-modulation atomic force microscopy on a few-layer MoS₂ flake, revealing the presence of linearly aligned, atomic-scale ripples on MoS₂, highlighted by black arrows (color scale range: 5 Å). The height of the highlighted ripples ranges from 1 Å to 3 Å.

In order to overcome the limitations of LFM and tapping-mode AFM in terms of spatial resolution, we imaged the topography of exfoliated MoS₂ flakes via frequency-modulation atomic force microscopy (FM-AFM) [85] performed in the attractive tip-sample interaction regime (an approach which is frequently referred to as noncontact AFM, i.e. NC-AFM [86]). The experiments were conducted using a customized JSPM-5100 microscope at McGill University. The microscope was equipped with a custom-made sample stage operating in high vacuum ($\sim 10^{-7}$ mbar). Ultra-sharp gold-coated tips (Adama Innovations AD-2.8-SS, tip radius, $r < 5$ nm, stiffness, $k = 2.0$ N/m) were employed and the microscope was controlled with the GXSM control module, with the implementation of active drift control. Nanosurf EasyPLL Plus was used for frequency shift detection. The cantilever was oscillated at its first resonance frequency, $f_0 = 61,786.3$ kHz, with an oscillation amplitude of 10 nm for all experiments. The sensitivity and the noise floor of the cantilever were calibrated with the thermal excitation technique in a quiet room. The measurements

were performed on as-exfoliated MoS₂ flakes, with no additional preparation under vacuum.

The utilization of ultra-sharp probes, combined with the fact that tip-sample contact is avoided during the measurements, finally resulted in the direct imaging of ripples on the MoS₂ surface (on a flake of ~ 65 Å height, corresponding to ~ 10 layers) in the form of linearly aligned, minute undulations in the surface topography, with out-of-plane corrugations of $1 - 5$ Å and lateral spacings on the order of $300 - 400$ Å (Figure 3.1c). These results, which constitute the first direct imaging of atomic-scale ripples on a 2D material such as MoS₂, at the same time open up the way for their detailed characterization in the form of interaction forces and energies, as reported in the next section.

3.3 Three-dimensional Interaction Spectroscopy of Atomic-scale Ripples on MoS₂

Three-dimensional atomic force microscopy (3D-AFM) is a well-established technique, the details of which can be found elsewhere [18,87]. We implemented constant frequency shift experiments to image the surface topography with different frequency set points. Imaging the same area of the sample at different heights leads to an "imaging volume". We established our imaging volume with 106 layers. Using established methods, we merged all topography and frequency shift data to reconstruct the three-dimensional potential energy landscape of the sample [88], with sub-nm lateral resolution. The lateral force acting on the tip was calculated via the negative gradient of the potential energy along the lateral direction [87]. Similarly, the vertical tip-sample interaction force was recovered with the negative gradient of the potential energy along the vertical direction. We rigorously checked the reconstructed tip-sample interaction data to make sure that it is well-posed [89,90].

While the presence of atomic-scale ripples on the MoS₂ samples (Figure 3.1c) may initially appear as a purely structural feature, it is important to probe their effect on the interactions that the 2D material exhibits with other bodies in its vicinity, in particular due to the potentially defining role they play in intriguing nanoscale mechanical characteristics such as friction anisotropy that is the subject of this chapter.

Motivated by this line of argument, we performed three-dimensional force / energy spectroscopy [18,87] on the MoS₂ flake of Figure 3.1c to extract the tip-sample interaction landscape in the form of three-dimensional, volumetric maps of interaction energies and forces, with meV- and pN-level resolution, respectively. The data, collected in the form of 106 constant-frequency-shift topography maps at different tip-sample distances via FM-AFM (Figure 3.2a), are combined to reconstruct the three-dimensional interaction force / energy volume. Subsequently, two-dimensional maps of tip-sample interaction energy at fixed tip-sample distances are extracted from the three-dimensional data (Figure 3.2b-f), which allows a high-resolution study

of how ripples modulate the tip-sample interaction landscape both spatially and energetically. The analysis of the data reveals that the mean energy corrugation associated with the ripples increases with decreasing tip-sample distance, from 5 meV to 30 meV over nearly 6 nm. This trend, which also points to an increasing magnitude of lateral forces experienced by the AFM tip near the ripples at decreasing tip-sample distances (which are proportional to the lateral gradient of the interaction energy in the scanning direction), demonstrates the non-negligible effect of atomic-scale ripples on mechanical characteristics of MoS₂ probed by recording tip-sample interactions in AFM experiments.

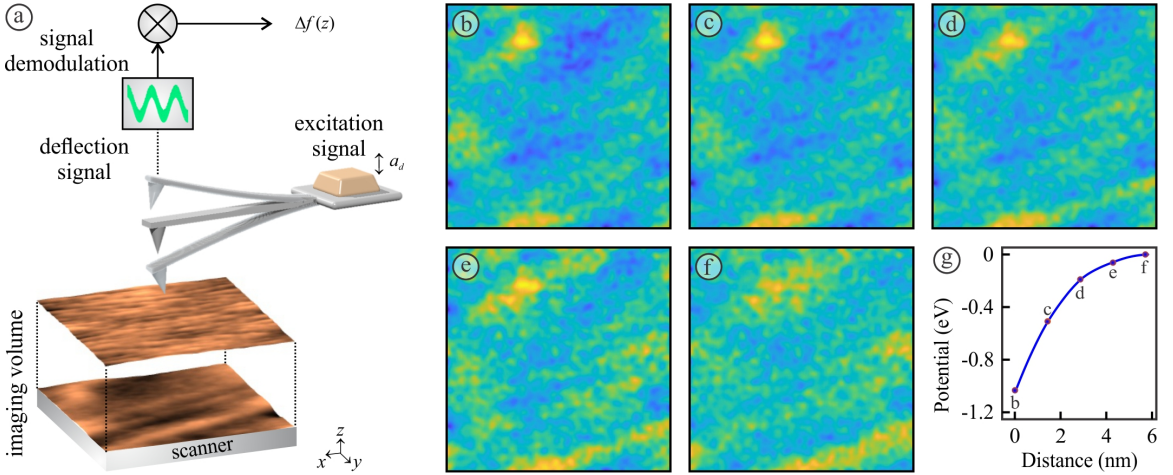


Figure 3.2: (a) Schematic demonstrating the surface topography being imaged at varying tip-sample distances by changing the frequency shift (Δf_0) of the AFM. The oscillation amplitude of the cantilever is kept constant at 10 nm by employing an active feedback of excitation signal, ad . Three-dimensional topography and resonance frequency shift data are utilized to reconstruct tip-sample interaction potential. (b-f) Maps of tip-sample interaction energy at different tip-sample distances recorded over the same location as in Figure 3.1c. The average tip-sample interaction energy at each tip-sample distance was subtracted from the data to highlight corrugations. The color scale range decreases from 87 meV in (b) to 7 meV in (f). (g) Average tip-sample interaction energy as a function of tip-sample distance. The tip-sample distances and the average tip-sample interaction energies corresponding to the data presented in (b) to (f) are highlighted on the plot.

3.4 Friction Anisotropy on MoS₂

Considering that the direction dependence, i.e. anisotropy, of friction can be potentially an important design parameter for 2D-material-based solid lubrication in small-scale mechanical systems, we performed LFM measurements to probe friction anisotropy on MoS₂ flakes exfoliated onto SiO₂. Our work was additionally motivated

by previous reports of friction anisotropy on 2D materials including graphene and MoS₂, where 2- and 6-fold symmetries have been reported [78-81], as well as irregular anisotropic behavior [82]. While 2-fold anisotropic behavior was tentatively explained by the presence of ripples [78,79] or stripes formed by molecular adsorbates [80], 6-fold anisotropy was ascribed to the hexagonal symmetry of the atomic structure of the involved materials [81].

LFM experiments reported here were performed with a commercial AFM instrument (Asylum Research, Cypher VRS) under ambient conditions. MoS₂ flakes were deposited onto SiO₂ substrates by standard mechanical exfoliation from commercially available bulk crystals via adhesive tape. The measurements were conducted using diamond-like-carbon-coated and diamond-coated cantilevers (Budget Sensors ContDLC and Nanosensors CDT-CONTR, respectively), with normal spring constant values (0.90 N/m and 0.28 N/m, respectively) as determined by the Sader method [21] introduced in Section 1.5.1. During LFM measurements, the effective normal load was purely due to adhesion and the scanning direction was perpendicular to the cantilever main axis. Topography and lateral force maps were acquired at scanning rates of 1 to 2 Hz. In order to investigate friction anisotropy, i.e. record the dependence of friction forces on scanning direction, the sample was manually rotated around its surface normal by $\sim 30^\circ$ between each measurement shown in Figure 3.3, for a full cycle corresponding to $\sim 360^\circ$. The measurements focused on areas of a few micrometer-square to a few nanometer-square on few-layer regions of MoS₂ flakes (corresponding to less than 10 but more than 4 layers). Each anisotropy experiment (corresponding to a nearly full cycle of friction force measurements reported in each panel of Figure 3.3) was completed on the same day, in a continuous experimental run, in an attempt to minimize variations in tip and sample conditions. Friction force maps were constructed from forward and backward lateral force maps [19], whereby each map consisted of 256 scan lines. Friction force values (Figure 3.3b,c) and ratios of friction forces recorded on SiO₂ and MoS₂ (Figure 3.3a), reported for each rotation angle, are extracted from these maps. Specifically, multiple (in particular, four) regions in the corresponding friction maps are considered for each rotation angle; the mean friction force (and friction force ratio) values as well as corresponding standard deviations are derived from these. In order to minimize the potential effect of tip changes during larger scans, the friction force recorded on the SiO₂ substrate is used as a reference value and divided by the friction force recorded on MoS₂, resulting in friction force ratios (as reported in Figure 3.3a).

As reported in Figure 3.3, analysis of multiple LFM experiments performed in our laboratory, aimed at studying anisotropic friction on MoS₂, revealed that the results fall into three main categories: (i) anisotropic behavior with nearly 2-fold symmetry, as demonstrated by data acquired on a large ($8\ \mu\text{m} \times 8\ \mu\text{m}$) scan area (Figure 3.3a), (ii) anisotropic behavior with nearly 4-fold symmetry, as demonstrated by data acquired on a smaller ($50\ \text{nm} \times 50\ \text{nm}$) scan area (Figure 3.3b), and finally, (iii) non-periodic friction, as demonstrated by data acquired on a scan area of

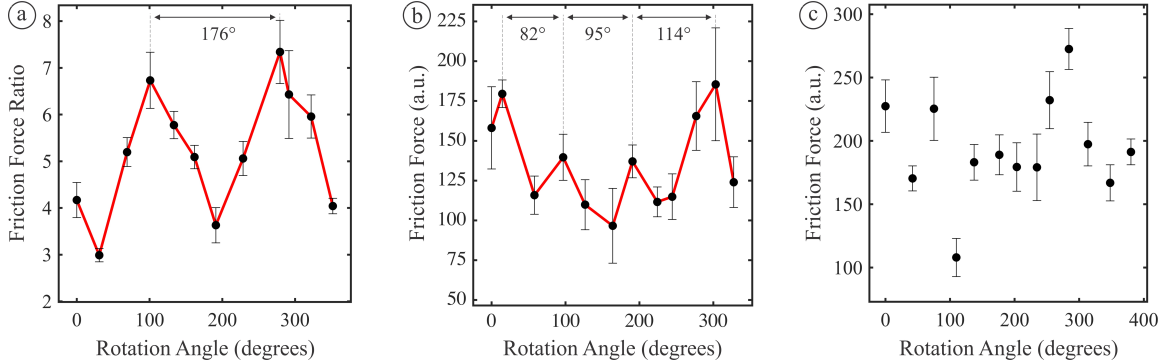


Figure 3.3: Friction anisotropy on MoS₂. (a) Ratios of friction forces recorded on SiO₂ and MoS₂, as a function of rotation angle, extracted from a scan of 8 μm × 8 μm in size. Periodic behavior with nearly 2-fold symmetry is observed. (b) Friction force recorded on MoS₂ as a function of rotation angle, extracted from a scan of 50 nm × 50 nm in size. Periodic behavior with nearly 4-fold symmetry is observed. (c) Friction force recorded on MoS₂ as a function of rotation angle, extracted from a scan of 1.5 μm × 1.5 μm in size, showing non-periodic character.

1.5 μm × 1.5 μm in size (Figure 3.3c). No experiments performed on scan areas smaller than 1.5 μm × 1.5 μm featured 2-fold anisotropy, while the largest scan area on which higher-symmetry anisotropy was recorded was 50 nm × 50 nm. Anisotropy ratios (the ratio between the highest and lowest friction values recorded in a ~ 360° cycle) for the experiments were 2.0 ± 0.4 , in the range of previously reported values for graphene and MoS₂ [78,82].

Despite the fact that the imaging of linearly aligned ripples on MoS₂ via our high-resolution AFM experiments can be utilized to explain the widely-reported observation of 2-fold friction anisotropy, the presence of higher-symmetry anisotropies in smaller scan sizes, as well as the observation of non-periodic friction, highlight the need for a more thorough evaluation of the effect of ripples on friction anisotropy.

Motivated as above, we performed a Fourier transform analysis on the two-dimensional lateral force maps derived from the volumetric interaction energy data. In particular, we calculated the relative probability of encountering a type of spatial symmetry (2-, 3-, 4-, 6-fold as well as no symmetry) on areas ranging in size from 16 nm × 16 nm to 250 nm × 250 nm that are scanned over whole lateral force maps (Figure 3.4). The results demonstrate that the effect of ripples on lateral force anisotropy (in the form of a 2-fold symmetry) is most dominant at larger scan sizes, while the chances of encountering 2-fold anisotropic behavior rapidly decrease at smaller scan sizes, where the "no symmetry" state dominates.

These results can be understood when one takes the finite lateral size and spacing of the ripples into account, the latter of which is in the range of 100s of Å. As such, in order for the ripples to have a noticeable influence on friction anisotropy, scan sizes need to be relatively larger, a conclusion that is supported by the friction

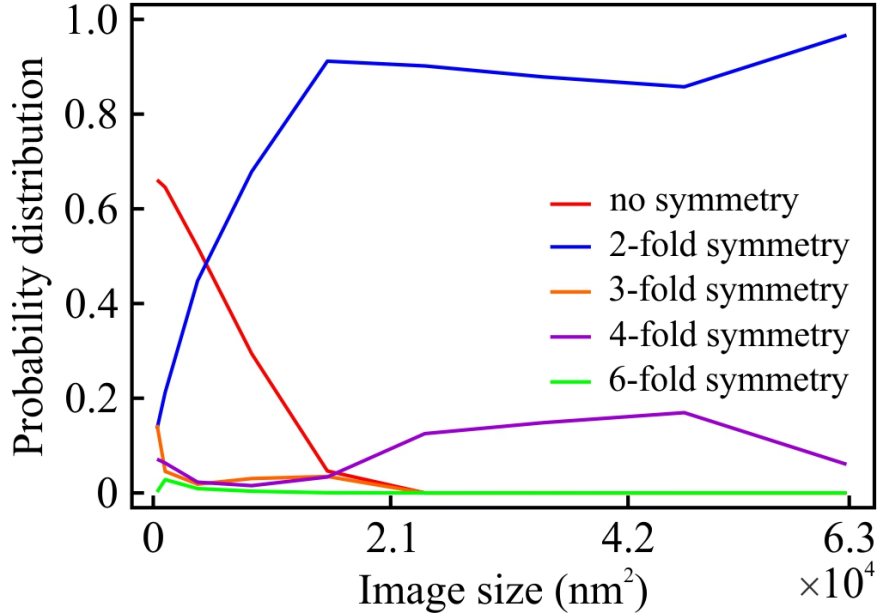


Figure 3.4: Dependence of friction anisotropy on scan size. The relative probabilities of encountering a particular type of spatial symmetry (2-, 3-, 4-, 6-fold as well as no symmetry at all) on lateral force maps derived from the three-dimensional potential energy data presented in Figure 3.2, as a function of scan size (ranging from 256 nm² to 62,500 nm²). While 2-fold symmetry, due to the presence of ripples, dominates the probability distribution at large scan sizes, the “no symmetry” state is dominant for smaller scans. A non-negligible observation of 4-fold symmetry for large scan sizes can be potentially attributed to the presence of surface structures other than linearly aligned ripples.

anisotropy experiments reported here, where no experiments performed on scan areas smaller than $1.5\ \mu\text{m} \times 1.5\ \mu\text{m}$ featured 2-fold anisotropy. This conclusion also shows that the observation of 2-fold friction anisotropy in certain prior reports [78,79] is definitely expected, based on the fact that the reported measurements were performed on areas of multiple μm in lateral size.

On the other hand, it needs to be understood that the predication of “no symmetry” for small scans, delivered by the present Fourier-transform-based analysis, is limited by the fact that the lateral force map analyzed here was acquired over an area of $250\ \text{nm} \times 250\ \text{nm}$. As such, the map lacks atomic-scale spatial resolution and thus cannot capture the effect of the hexagonal symmetry of atomic-scale structure on friction anisotropy. In fact, for LFM data acquired over small areas, it is natural to expect that the hexagonal symmetry of the atomic structure will result in an anisotropic behavior closer to 6-fold symmetry. Consequently, the convolution of this effect with the still non-negligible influence of ripples on scan areas of a few tens of nm in lateral size, results in anisotropic behavior with an intermediate level of symmetry (such as the measurement reported in Figure 3.3b that features nearly

4-fold anisotropy). At the other end of the spectrum, once scans are limited only to a few nm in lateral size, the influence of ripples completely disappears, and the emergence of 6-fold anisotropic behavior is expected, as clearly demonstrated by experiments performed on graphene [81].

Despite the fact that the discussion above sheds light on the observation of 2-fold and higher order anisotropic behavior of friction exhibited by 2D materials, the frequent observation of non-periodic friction data (Figure 3.3c) needs to be explained, too. While tip apex changes during experiments (that are known to directly affect the magnitude of friction forces during LFM measurements [45]) can be held responsible for such results, we alternatively ascribe the occasional inability to record clearly anisotropic friction data to the fact that the presence and distribution of ripples on the MoS₂ flakes appear to be non-uniform, with significant areas on the flakes that are devoid of linearly aligned ripples (Figure 3.5). As the atomic-scale ripples cannot be imaged during the LFM measurements, it is conceivable that some measurements are ultimately performed on areas with no linearly aligned ripples, resulting in non-periodic results in terms of friction anisotropy.

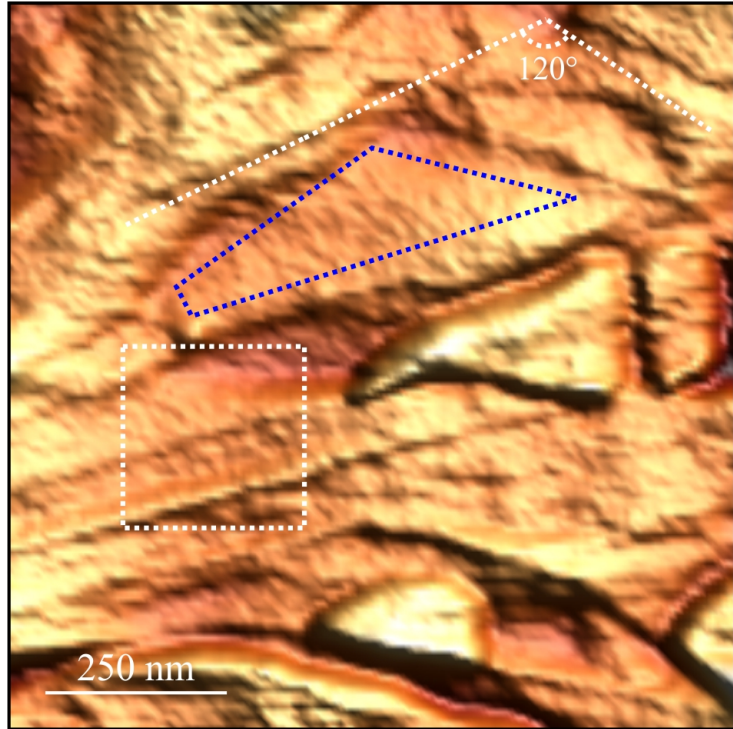


Figure 3.5: A large-scale (1,000 nm \times 1,000 nm) topographical image (in isometric, pseudo-3D form; color scale range: 4.2 nm) of the MoS₂ flake acquired via high-resolution FM-AFM, including the region with linearly aligned ripples investigated in Figs. 3.1c and 3.2 (dashed white rectangle), a representative region where there are no discernible ripples (area highlighted with the blue dashed lines) and a ripple that changes direction by $\sim 120^\circ$ (dashed white lines), in accordance with the atomic symmetry of MoS₂.

Finally, it needs to be mentioned that our experiments did not yield any evidence for linearly aligned structures formed by adsorbed molecules as proposed by Gallagher et al. [80], even when the MoS₂ surfaces were imaged by the high-resolution NC-AFM approach. Along a similar line of thought, in order to rule out that the linearly aligned structures we observe are indeed intrinsic ripples of MoS₂ and not clusters of adsorbates on the MoS₂ flakes, we studied energy dissipation maps acquired simultaneously with the other data channels during NC-AFM imaging (Figure 3.6). The absence of a discernible contrast in such maps supports the conclusions reached about the nature of the atomic-scale structures we observe as intrinsic ripples.

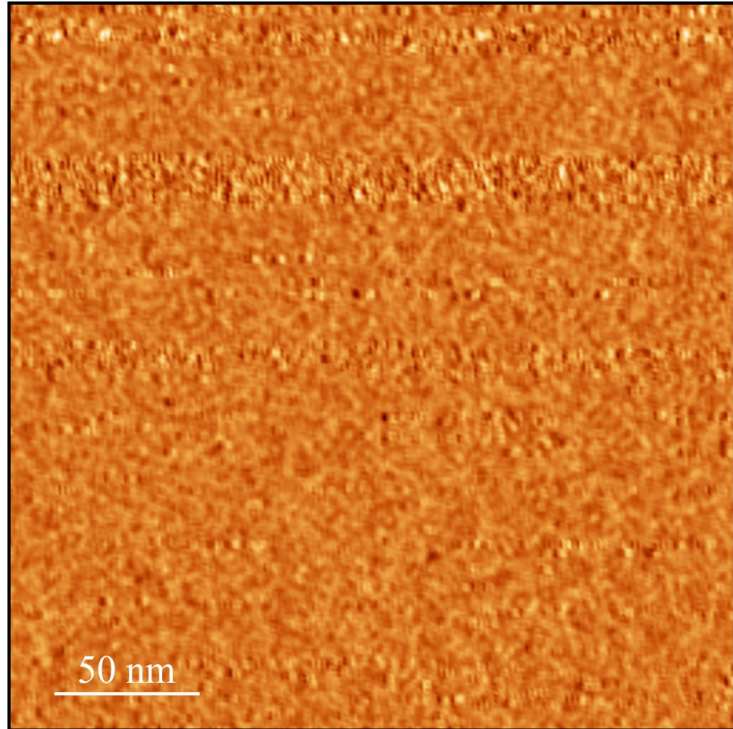


Figure 3.6: A map (250 nm \times 250 nm) of energy dissipation recorded simultaneously with the high-resolution topographical image of Figure 3.1c (color scale range: 1.8 meV). The lack of contrast demonstrates that the ripples observed in the topography map are indeed inherent structural features and not clusters formed by adsorbates from the environment.

In this chapter, we presented high-resolution AFM experiments that led to the direct imaging of atomic-scale ripples on few-layer flakes of MoS₂. Three-dimensional force / energy spectroscopy showed the extent to which the presence of the ripples influences the interactions of MoS₂ with the probing tip. Our experiments directly revealed the presence of linearly aligned ripples as the fundamental physical mechanism responsible for the direction-dependence of friction on 2D materials, and also allowed the explanation of the wide variety of anisotropic behavior observed on such materials as a function of scan size. Further experiments, potentially performed

with probes that are themselves single- or few-layers of 2D materials [91], need to be performed to more accurately ascertain the impact of ripples on 2D-material-based solid lubrication in micro- and nano-scale mechanical systems. The results reported in this chapter have been submitted in the form of a journal article and are now under review.

Chapter 4

Nanotribology of Re-Doped MoS₂

4.1 Dependence of Friction on Number of Layers

As mentioned in previous parts of this thesis, MoS₂ has been extensively studied for a multitude of electronic and mechanical applications. For instance, to develop next-generation nanodevices such as nanoscale data storage systems and nano electro-mechanical systems (NEMS), the mechanical properties of atomically thin materials need to be quantitatively studied and well understood. In particular, certain aspects of the nanoscale tribology of MoS₂ have been previously explored with AFM measurements under various conditions [43,61,68,79]. One of the important questions in the nanotribology on 2D materials involves the effect of thickness (i.e. number of layers) on the measured friction force.

Lee et al., in their milestone paper published in 2010 [43], state that AFM-based friction measurements on 2D materials are dominated by the “puckering” effect. This effect manifests in the form of a “pucker” that forms in front of a sharp AFM tip that slides (i.e. plows) on a thin sheet of material (Figure 4.1). This pucker increases the contact area and causes high adhesion forces between tip and sample, consequently leading to an enhancement of the friction force. As the number of layers of a given 2D material increases, so does the out-of-plane bending stiffness, which ultimately leads to a suppression of puckering and a decrease in the friction force. As a result, it is expected to see remarkably higher friction on a single-layer sheet in comparison to few-layers. This layer-dependent friction trend was observed experimentally in several studies on graphene, MoS₂, hexagonal boron nitride (h-BN) and niobium diselenide (NbSe₂), on different substrates such as silicon, mica and h-BN [43,44,92,93].

Despite the seemingly universal trend of decreasing friction with increasing number of layers for 2D materials, an open question is whether this trend can be suppressed or even reversed under certain conditions. Taking this open question into account, and additionally considering the lack of nanotribology work on chemically doped MoS₂ samples in the literature, we present in this chapter the first results of AFM-based nanotribology work performed on Re-doped MoS₂. These measurements

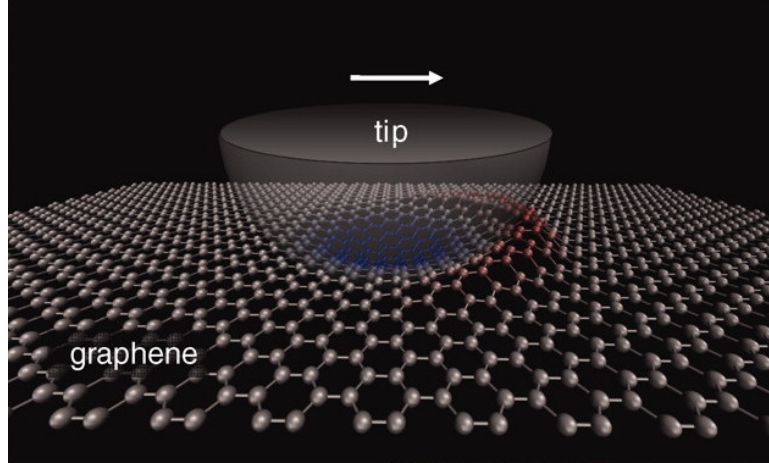


Figure 4.1: Illustration of the formation of a "pucker" in front of an AFM probe tip sliding on single-layer graphene [43]. Similar mechanisms are believed to occur during the investigation of other 2D materials, including MoS₂.

allow us to study the tribological properties of Re-doped MoS₂ in terms of layer dependence of friction, adhesion measurements on single-layer and few-layer flakes, and lubricative performance in comparison to undoped MoS₂.

The Re-doped MoS₂ samples investigated here have been provided by the research group of Prof. Sefaattin Tongay at Arizona State University in the form of bulk crystals. The standard method of mechanical exfoliation has been utilized to deposit single- and few-layer flakes of both Re-doped and undoped MoS₂ on SiO₂ substrates. The measurements were performed using a commercial AFM instrument (Asylum Research, Cypher VRS). During the recording of friction force maps, the effective normal load was purely due to adhesion and the scanning direction was perpendicular to the cantilever main axis. Topography and lateral force maps were acquired at scanning rates ranging from 1 to 2 Hz. Both Re-doped and undoped MoS₂ samples were characterized with the same AFM probe to compare nanotribological properties with minimal influence of probe changes. The thickness of the flakes were determined from AFM topography maps. If the height for a given region was less than the minimum height for bi-layer MoS₂ (~ 1.3 nm), it was evaluated as single-layer.

4.1.1 Undoped MoS₂

The layer-dependence results obtained via friction force maps recorded on undoped MoS₂ are in harmony with previous experimental studies in the literature [43]. In particular, as demonstrated in Figure 4.2, the friction force is decreasing with increasing number of layers, meaning that the sharp tip apex experiences high friction on single layer MoS₂ and the force decreases monotonically with thickness due to the well-known puckering effect.

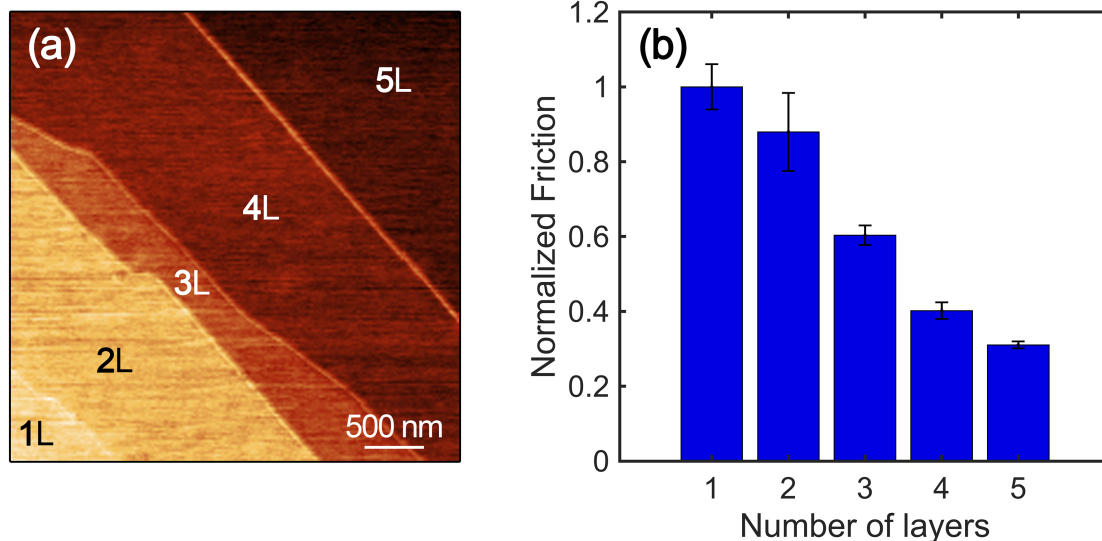


Figure 4.2: (a) Friction force map of an undoped MoS₂ flake with 1, 2, 3, 4, and 5 layers, situated on a SiO₂ substrate. (b) Friction on MoS₂ areas with different layer thicknesses. Friction is normalized to the value obtained on the 1L area.

4.1.2 Re-doped MoS₂

As opposed to undoped MoS₂, AFM-based friction measurements on Re-doped MoS₂ surprisingly revealed that Re-doped flakes exhibit a completely unexpected, i.e. anomalous layer dependence of friction. In particular, results reported in Figure 4.3 show a striking contrast to those in Figure 4.2. Specifically, single-layer Re-doped MoS₂ exhibits the lowest friction force and the friction force increases with the number of layers, in violation of the well-known puckering effect.

In order to confirm these results and ensure that the findings are not due to an exceptional flake, measurements were repeated on a different Re-doped MoS₂ flake with varying layer thicknesses. The results obtained on this flake, summarized in Figure 4.4, demonstrate a similar trend, with increasing friction for higher number of layers. Once again, this finding reveals a significant deviation from the literature, one that can be defined as an anomalous / inverse layer-dependence of friction. It should be mentioned that an increasing friction trend with increasing number of layers was shown only once before, on undoped MoS₂ samples [92], and attributed to an exceptionally large probe apex. However, the “regular” results obtained on undoped MoS₂ using the same cantilever probe in our experiments (Figure 4.2) exclude a possible link between probe characteristics and the unusual findings on Re-doped MoS₂. It also needs to be emphasized that the measurements were repeated multiple times on different days, with the same trends observed on undoped and Re-doped samples. Hence we are confident that the observed anomalous trend is intrinsic to Re-doped MoS₂ and not probe-dependent.

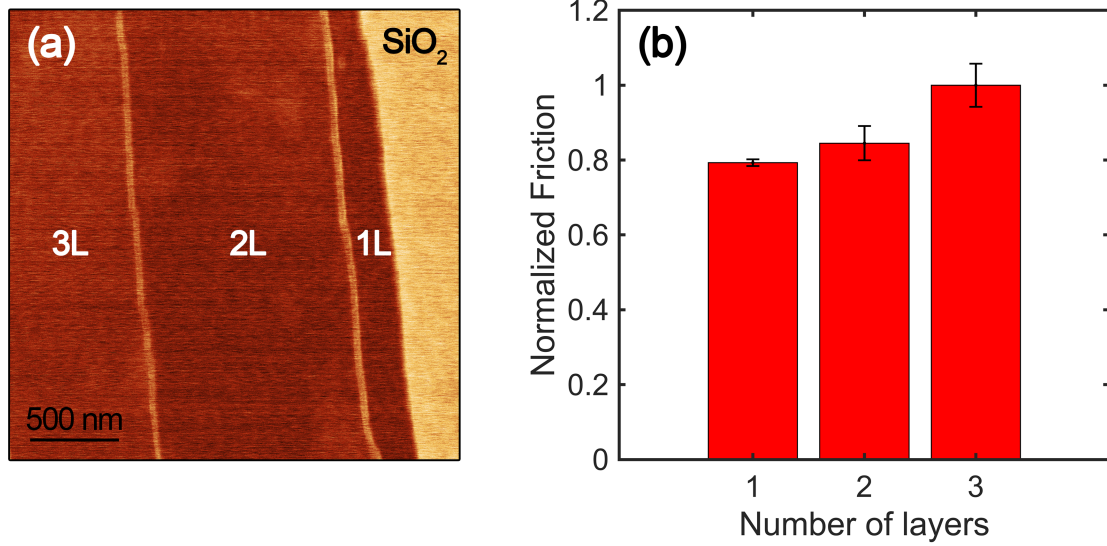


Figure 4.3: (a) Friction force map obtained on a Re-doped MoS₂ flake with 1, 2, and 3 layers, situated on a SiO₂ substrate. (b) Friction on Re-doped MoS₂ areas with different layer thicknesses. Friction is normalized to the value obtained on the 3L area.

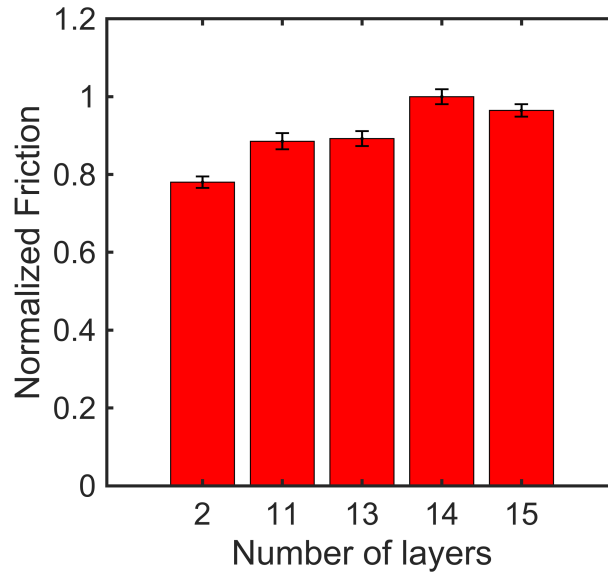


Figure 4.4: Friction force values measured on 2, 11, 13, 14, and 15 layers of Re-doped MoS₂ on a SiO₂ substrate. Friction is normalized to the value obtained on the 14L sample (i.e. the maximum friction value).

4.2 Roughness Measurements

In order to try and identify the physical mechanism responsible for the observation of anomalous layer-dependence of friction on Re-doped MoS₂ samples,

we initially performed AFM-based roughness measurements in contact mode. In particular, Figure 4.5a shows roughness measurements on undoped MoS₂. While mean roughness values recorded on 1-, 2- and 3-layer regions are nearly identical, the roughness of the bulk region is $\sim 11\%$ lower, in accordance with previous studies that proposed reduced roughness at increasing number of layers as an alternative / complementary mechanism to the puckering effect [46]. On the other hand, the roughness measurements performed on Re-doped MoS₂ (reported in Figure 4.5b) show no significant change between different regions, with the percent difference between reported roughness values with different number of layers on Re-doped MoS₂ being less than $\sim 2.2\%$. These findings demonstrate that changing roughness with increasing number of layers cannot be the reason behind the the observation of anomalous layer-dependence of friction on Re-doped MoS₂ samples.

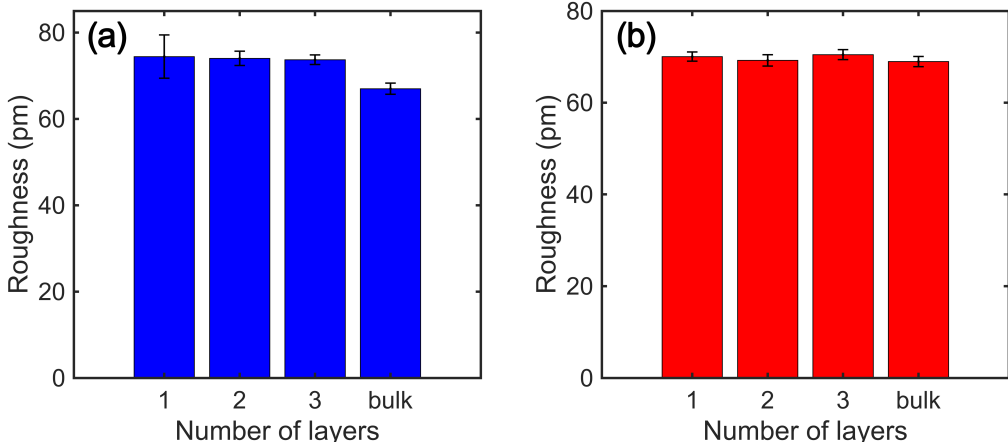


Figure 4.5: Roughness values measured on 1-, 2-, 3-layer and bulk regions of (a) undoped MoS₂, and (b) Re-doped MoS₂ extracted from 10 nm \times 10 nm scans.

4.3 Adhesion Measurements

An alternative physical mechanism potentially responsible for the observation of anomalous layer-dependence of friction on Re-doped MoS₂ samples could involve increasing adhesion (and thus, friction) at increasing number of layers. Consequently, in order to probe whether there is any effect of number of layers on adhesion force, we performed force spectroscopy experiments on undoped and Re-doped MoS₂ samples to extract adhesion values. As seen in Figure 4.6a, an overall decreasing (but not always monotonic) trend in adhesion force is observed from single-layer to bulk on undoped MoS₂. In particular, adhesion is decreased from single-layer to bilayer MoS₂ and then increased. After reaching 3 layers of thickness, adhesion decreases monotonically with increasing thickness. In particular, bilayer undoped MoS₂ showed $\sim 25\%$ lower adhesion than single-layer, while friction on the 3-layer was $\sim 15\%$ lower than the

single-layer sheet. Four-layer and bulk sheets showed $\sim 23\%$ and $\sim 29\%$ lower adhesion than the single layer, respectively.

For Re-doped MoS_2 , as it is seen in Figure 4.6b, a monotonically decreasing adhesion trend with increasing number of layers is observed during the measurements. Bilayer Re-doped MoS_2 showed $\sim 1.5\%$ lower adhesion than the single-layer sheet, while adhesion on 3-layer and bulk sheets was measured to be $\sim 11\%$ and $\sim 21\%$ lower than the single-layer sheet, respectively. Thus, on both types of materials, i.e. undoped and Re-doped MoS_2 , bulk sheets showed somewhere between $\sim 20\%$ and $\sim 30\%$ lower adhesion than the single-layer sheet. As the results are generally consistent between the two types of samples, adhesion trends cannot explain the anomalous friction trend observed on Re-doped MoS_2 .

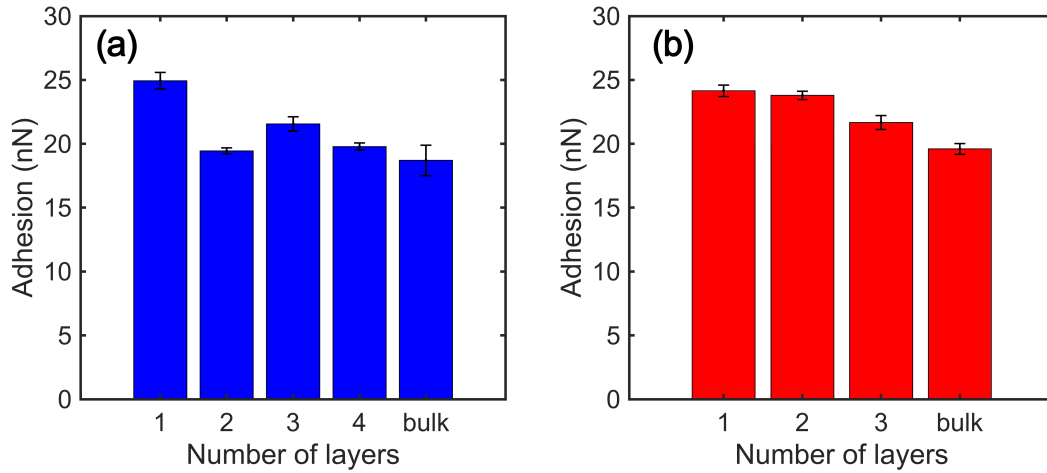


Figure 4.6: Adhesion force values measured on (a) 1-, 2-, 3-, 4-layer and bulk regions of undoped MoS_2 , and (b) 1-, 2-, and 3-layer and bulk regions of Re-doped MoS_2 .

While the results reported in this chapter are scientifically quite interesting, our attempts at elucidating the underlying mechanisms by roughness and adhesion measurements have not yielded the desired results. Consequently, theory support is now solicited to explain the anomalous layer dependence of friction on Re-doped MoS_2 , potentially focusing on the effect of Re doping on phonon vibration frequencies and density of states [94].

Chapter 5

Summary and Outlook

This thesis focused on the nanotribology of MoS₂ by taking advantage of state-of-the-art AFM measurements. For all experiments reported here, MoS₂ flakes were exfoliated onto SiO₂ substrates by standard mechanical exfoliation from bulk crystals via adhesive tape. All experiments were performed under ordinary laboratory conditions using a commercial AFM instrument (Asylum Research, Cypher VRS) by the utilization of diamond, diamond-like carbon and silicon cantilevers, except FM-AFM experiments reported in Chapter 3 that were performed by our collaborators at McGill University using a custom AFM system operating under high vacuum.

One of the missing parts of the puzzle in the literature was the speed dependence of friction on MoS₂. To address this gap in literature, we performed speed dependence experiments on single-layer and bulk MoS₂ flakes and thereby probed friction forces as a function of sliding speed. The results of the experiments demonstrated that (i) friction forces increase logarithmically with respect to sliding speed, (ii) there is no correlation between the speed dependence of friction and the number of layers of MoS₂, and (iii) changes in the speed dependence of friction can be attributed to changes in the physical characteristics of the AFM probe, manifesting in the form of varying contact stiffness and tip-sample interaction potential parameters in the thermally activated Prandtl–Tomlinson model. The findings reported in this part of the thesis (Chapter 2) and published in the form of a journal article [68], contributed to the ongoing formation of a mechanistic understanding of the speed dependence of nanoscale friction on two-dimensional materials.

Another important milestone in establishing a comprehensive understanding of the nanotribology of MoS₂ involved the detection of atomic-scale ripples in few-layer flakes and analyzing the resulting direction dependence, i.e. anisotropy of friction. Toward this goal, high-resolution AFM experiments were performed to directly image atomic-scale ripples on few-layer MoS₂ in real space. Additionally, three-dimensional force/energy spectroscopy techniques were used to quantitatively study the effect of ripples on the tip-sample interaction landscape. Multiple symmetries were observed in friction force microscopy experiments which were explained by an interplay between rippled sample areas and scan size. The results of these experiments, reported in Chapter 3 and submitted in the form of a journal

article, open a new door to explain the universal anisotropic behavior of 2D materials [79] with the example of MoS₂.

Finally, in Chapter 4, the effect of chemical doping on the nanotribological properties of MoS₂ was investigated by way of AFM experiments performed on Re-doped MoS₂ flakes. In particular, an anomalous dependence of friction on the number of layers (i.e. increasing friction with increasing number of layers) when compared with other 2D materials was observed. Comparative adhesion and roughness measurements performed on Re-doped and undoped MoS₂ flakes did not explain the anomalous layer dependence trend. Consequently, theory support is now solicited to explain the observed effect, potentially focusing on the effect of Re doping on phonon vibration frequencies and density of states [94].

Although the results reported in this thesis contributed substantially to forming a basic understanding of the nanotribology of MoS₂, several gaps in our knowledge still remain. In particular, it remains to be seen whether the anomalous layer dependence of friction observed on Re-doped MoS₂ would also be observed on MoS₂ samples doped with other elements and what mechanism specifically causes the inverse layer dependence. With respect to speed dependence experiments, measurements performed on MoS₂ flakes of intermediate thickness (e.g. bi- and tri-layer flakes) could reveal trends that were not observed on single-layer and bulk samples investigated in Chapter 2. More generally, the crucial role that the AFM probe plays in extracting the nanotribological properties of 2D materials needs to be more carefully monitored and assessed, perhaps by way of precise TEM measurements [95] performed before and after the experiments on the probe apexes.

Bibliography

- [1] Holmberg, K. & Erdemir, A. Influence of tribology on global energy consumption, costs and emissions. *Friction* **5**, 263–284 (2017).
- [2] Martin, J. M. & Erdemir, A. Superlubricity: Friction’s vanishing act. *Phys. Today* **71**, 40–46 (2018).
- [3] Nosonovsky, M. Oil as a Lubricant in the Ancient Middle East. *Tribol. Online* **2**, 44–49 (2007).
- [4] Berna, F. *et al.* Microstratigraphic evidence of in situ fire in the Acheulean strata of Wonderwerk Cave, Northern Cape province, South Africa. *Proc. Natl. Acad. Sci.* **109**, E1215–E1220 (2012).
- [5] Dowson, D. *History of Tribology, Second Edition.* (Professional Engineering Publishing, London, 1998).
- [6] Bhushan, B. *Principles and Applications of Tribology, Second Edition.* (Wiley, New York, 1999). doi:10.1002/9781118403020.
- [7] Bhushan, B. *Introduction to Tribology, Second Edition.* (Wiley, New York, 2013). doi:10.1002/9781118403259.
- [8] Vinci, L. Da, Stern, R. & Manges, A. *Leonardo Da Vinci Master Draftsman: Catalogue to an Exhibition at The Metropolitan Museum of Art, New York 2003.* (2003).
- [9] Amontons, M. De la resistance cause’e dans les machines. *Mem. l’Academie R. des Fr.* (1699).
- [10] Tabor, D. & Winterton, R. H. S. Surface Forces: Direct Measurement of Normal and Retarded van der Waals Forces. *Nature* **219**, 1120–1121 (1968).
- [11] Krim, J. Surface science and the atomic-scale origins of friction: what once was old is new again. *Surf. Sci.* **500**, 741–758 (2002).
- [12] Szlufarska, I., Chandross, M. & Carpick, R. W. Recent advances in single-asperity nanotribology. *J. Phys. D. Appl. Phys.* **41**, 123001 (2008).

- [13] Binnig, G., Quate, C. F. & Gerber, C. Atomic Force Microscope. *Phys. Rev. Lett.* **56**, 930–933 (1986).
- [14] Schirmeisen, A. & Schwarz, U. D. Measuring the Friction of Nanoparticles: A New Route towards a Better Understanding of Nanoscale Friction. *ChemPhysChem* **10**, 2373–2382 (2009).
- [15] Binnig, G., Rohrer, H., Gerber, C. & Weibel, E. Surface Studies by Scanning Tunneling Microscopy. *Phys. Rev. Lett.* **49**, 57–61 (1982).
- [16] First atomic force microscope, United States, 1985 | Science Museum Group Collection. <https://collection.sciencemuseumgroup.org.uk>.
- [17] Eaton, P. & West, P. *Atomic Force Microscopy*. (Oxford University Press, 2010). doi:10.1093/acprof:oso/9780199570454.001.0001.
- [18] Baykara, M. Z., Schwendemann, T. C., Altman, E. I. & Schwarz, U. D. Three-Dimensional Atomic Force Microscopy - Taking Surface Imaging to the Next Level. *Adv. Mater.* **22**, 2838–2853 (2010).
- [19] Schwarz, U. D., Köster, P. & Wiesendanger, R. Quantitative analysis of lateral force microscopy experiments. *Rev. Sci. Instrum.* **67**, 2560–2567 (1996).
- [20] Sader, J. E., Larson, I., Mulvaney, P. & White, L. R. Method for the calibration of atomic force microscope cantilevers. *Rev. Sci. Instrum.* **66**, 3789–3798 (1995).
- [21] Sader, J. E., Chon, J. W. M. & Mulvaney, P. Calibration of rectangular atomic force microscope cantilevers. *Rev. Sci. Instrum.* **70**, 3967–3969 (1999).
- [22] Palacio, M. L. B. & Bhushan, B. Normal and Lateral Force Calibration Techniques for AFM Cantilevers. *Crit. Rev. Solid State Mater. Sci.* **35**, 73–104 (2010).
- [23] Varenberg, M., Etsion, I. & Halperin, G. An improved wedge calibration method for lateral force in atomic force microscopy. *Rev. Sci. Instrum.* **74**, 3362–3367 (2003).
- [24] Ogletree, D. F., Carpick, R. W. & Salmeron, M. Calibration of frictional forces in atomic force microscopy. *Rev. Sci. Instrum.* **67**, 3298–3306 (1996).
- [25] Cappella, B. & Dietler, G. Force-distance curves by atomic force microscopy. *Surf. Sci. Rep.* **34**, 1–104 (1999).
- [26] Novoselov, K. S. Electric Field Effect in Atomically Thin Carbon Films. *Science* **306**, 666–669 (2004).

- [27] Wang, Q. H., Kalantar-Zadeh, K., Kis, A., Coleman, J. N. & Strano, M. S. Electronics and optoelectronics of two-dimensional transition metal dichalcogenides. *Nat. Nanotechnol.* **7**, 699–712 (2012).
- [28] Das, S., Robinson, J. A., Dubey, M., Terrones, H. & Terrones, M. Beyond Graphene: Progress in Novel Two-Dimensional Materials and van der Waals Solids. *Annu. Rev. Mater. Res.* **45**, 1–27 (2015).
- [29] Novoselov, K. S., Mishchenko, A., Carvalho, A. & Castro Neto, A. H. 2D materials and van der Waals heterostructures. *Science* **353**, aac9439 (2016).
- [30] Akinwande, D. *et al.* A review on mechanics and mechanical properties of 2D materials—Graphene and beyond. *Extrem. Mech. Lett.* **13**, 42–77 (2017).
- [31] Chhowalla, M. *et al.* The chemistry of two-dimensional layered transition metal dichalcogenide nanosheets. *Nat. Chem.* **5**, 263–275 (2013).
- [32] Ganatra, R. & Zhang, Q. Few-Layer MoS₂: A Promising Layered Semiconductor. *ACS Nano* **8**, 4074–4099 (2014).
- [33] Jariwala, D., Sangwan, V. K., Lauhon, L. J., Marks, T. J. & Hersam, M. C. Emerging Device Applications for Semiconducting Two-Dimensional Transition Metal Dichalcogenides. *ACS Nano* **8**, 1102–1120 (2014).
- [34] Akinwande, D., Petrone, N. & Hone, J. Two-dimensional flexible nanoelectronics. *Nat. Commun.* **5**, 5678 (2014).
- [35] Oviedo, J. P. *et al.* In Situ TEM Characterization of Shear-Stress-Induced Interlayer Sliding in the Cross Section View of Molybdenum Disulfide. *ACS Nano* **9**, 1543–1551 (2015).
- [36] Bertolazzi, S., Brivio, J. & Kis, A. Stretching and Breaking of Ultrathin MoS₂. *ACS Nano* **5**, 9703–9709 (2011).
- [37] Lee, C., Wei, X., Kysar, J. W. & Hone, J. Measurement of the Elastic Properties and Intrinsic Strength of Monolayer Graphene. *Science* **321**, 385–388 (2008).
- [38] Zhang, P. *et al.* Fracture toughness of graphene. *Nat. Commun.* **5**, 3782 (2014).
- [39] Molybdenum Disulfide, MoS₂: Theory, Structure & Applications | Ossila.
<https://www.ossila.com/pages/molybdenum-disulfide-mos2>.
- [40] Kim, K.-S. *et al.* Chemical Vapor Deposition-Grown Graphene: The Thinnest Solid Lubricant. *ACS Nano* **5**, 5107–5114 (2011).
- [41] Berman, D., Erdemir, A. & Sumant, A. V. Graphene: a new emerging lubricant. *Mater. Today* **17**, 31–42 (2014).

- [42] Berman, D., Erdemir, A. & Sumant, A. V. Approaches for Achieving Superlubricity in Two-Dimensional Materials. *ACS Nano* **12**, 2122–2137 (2018).
- [43] Lee, C. *et al.* Frictional Characteristics of Atomically Thin Sheets. *Science* **328**, 76–80 (2010).
- [44] Egberts, P., Han, G. H., Liu, X. Z., Johnson, A. T. C. & Carpick, R. W. Frictional Behavior of Atomically Thin Sheets: Hexagonal-Shaped Graphene Islands Grown on Copper by Chemical Vapor Deposition. *ACS Nano* **8**, 5010–5021 (2014).
- [45] Demirbaş, T. & Baykara, M. Z. Nanoscale tribology of graphene grown by chemical vapor deposition and transferred onto silicon oxide substrates. *J. Mater. Res.* **31**, 1914–1923 (2016).
- [46] Ye, Z., Balkanci, A., Martini, A. & Baykara, M. Z. Effect of roughness on the layer-dependent friction of few-layer graphene. *Phys. Rev. B* **96**, 115401 (2017).
- [47] Tripathi, M. *et al.* Friction and Adhesion of Different Structural Defects of Graphene. *ACS Appl. Mater. Interfaces* **10**, 44614–44623 (2018).
- [48] Lavini, F. *et al.* Friction and work function oscillatory behavior for an even and odd number of layers in polycrystalline MoS₂. *Nanoscale* **10**, 8304–8312 (2018).
- [49] Vazirisereshk, M. R. *et al.* Origin of Nanoscale Friction Contrast between Supported Graphene, MoS₂, and a Graphene/MoS₂ Heterostructure. *Nano Lett.* **19**, 5496–5505 (2019).
- [50] Schumacher, A. Influence of humidity on friction measurements of supported MoS₂ single layers. *J. Vac. Sci. Technol. B Microelectron. Nanom. Struct.* **14**, 1264 (1996).
- [51] Chen, Z., He, X., Xiao, C. & Kim, S. Effect of Humidity on Friction and Wear—A Critical Review. *Lubricants* **6**, 74 (2018).
- [52] Gould, S. G. & Roberts, E. W. In-vacuo torque performance of dry-lubricated ball bearings and cryogenic temperatures. in *Proceedings of the 23rd Aerospace Mechanisms Symp* 319 (NASA, 1989).
- [53] Ptak, F., Almeida, C. M. & Prioli, R. Velocity-dependent friction enhances tribomechanical differences between monolayer and multilayer graphene. *Sci. Rep.* **9**, 14555 (2019).
- [54] Gnecco, E. *et al.* Velocity Dependence of Atomic Friction. *Phys. Rev. Lett.* **84**, 1172–1175 (2000).

- [55] Riedo, E., Gnecco, E., Bennewitz, R., Meyer, E. & Brune, H. Interaction Potential and Hopping Dynamics Governing Sliding Friction. *Phys. Rev. Lett.* **91**, 084502 (2003).
- [56] Liu, X.-Z. *et al.* Dynamics of Atomic Stick-Slip Friction Examined with Atomic Force Microscopy and Atomistic Simulations at Overlapping Speeds. *Phys. Rev. Lett.* **114**, 146102 (2015).
- [57] Jansen, L., Hölscher, H., Fuchs, H. & Schirmeisen, A. Temperature Dependence of Atomic-Scale Stick-Slip Friction. *Phys. Rev. Lett.* **104**, 256101 (2010).
- [58] Zwörner, O., Hölscher, H., Schwarz, U. D. & Wiesendanger, R. The velocity dependence of frictional forces in point-contact friction. *Appl. Phys. A Mater. Sci. Process.* **66**, S263–S267 (1998).
- [59] Chen, J., Ratera, I., Park, J. Y. & Salmeron, M. Velocity Dependence of Friction and Hydrogen Bonding Effects. *Phys. Rev. Lett.* **96**, 236102 (2006).
- [60] Ouyang, W. *et al.* Load and Velocity Dependence of Friction Mediated by Dynamics of Interfacial Contacts. *Phys. Rev. Lett.* **123**, 116102 (2019).
- [61] Vazirisereshk, M. R., Martini, A., Strubbe, D. A. & Baykara, M. Z. Solid Lubrication with MoS₂: A Review. *Lubricants* **7**, 57 (2019).
- [62] Voevodin, A. & Zabinski, J. Nanocomposite and nanostructured tribological materials for space applications. *Compos. Sci. Technol.* **65**, 741–748 (2005).
- [63] Li, H. *et al.* Optical Identification of Single- and Few-Layer MoS₂ Sheets. *Small* **8**, 682–686 (2012).
- [64] Sang, Y., Dubé, M. & Grant, M. Thermal Effects on Atomic Friction. *Phys. Rev. Lett.* **87**, 174301 (2001).
- [65] Schwarz, U. D. & Hölscher, H. Exploring and explaining friction with the prandtl-Tomlinson model. *ACS Nano* **10**, 38–41 (2016).
- [66] Dagdeviren, O. E. Exploring load, velocity, and surface disorder dependence of friction with one-dimensional and two-dimensional models. *Nanotechnology* **29**, 315704 (2018).
- [67] Dong, Y., Gao, H., Martini, A. & Egberts, P. Reinterpretation of velocity-dependent atomic friction: Influence of the inherent instrumental noise in friction force microscopes. *Phys. Rev. E* **90**, 012125 (2014).
- [68] Acikgoz, O. & Baykara, M. Z. Speed dependence of friction on single-layer and bulk MoS₂ measured by atomic force microscopy. *Appl. Phys. Lett.* **116**, 071603 (2020).

- [69] Mermin, N. D. Crystalline Order in Two Dimensions. *Phys. Rev.* **176**, 250–254 (1968).
- [70] Meyer, J. C. *et al.* The structure of suspended graphene sheets. *Nature* **446**, 60–63 (2007).
- [71] Fasolino, A., Los, J. H. & Katsnelson, M. I. Intrinsic ripples in graphene. *Nat. Mater.* **6**, 858–861 (2007).
- [72] Brivio, J., Alexander, D. T. L. & Kis, A. Ripples and Layers in Ultrathin MoS₂ Membranes. *Nano Lett.* **11**, 5148–5153 (2011).
- [73] Wang, W. L. *et al.* Direct Imaging of Atomic-Scale Ripples in Few-Layer Graphene. *Nano Lett.* **12**, 2278–2282 (2012).
- [74] Geringer, V. *et al.* Intrinsic and extrinsic corrugation of monolayer graphene deposited on SiO₂. *Phys. Rev. Lett.* **102**, 076102 (2009).
- [75] Morozov, S. V. *et al.* Strong Suppression of Weak Localization in Graphene. *Phys. Rev. Lett.* **97**, 016801 (2006).
- [76] Bao, W. *et al.* Controlled ripple texturing of suspended graphene and ultrathin graphite membranes. *Nat. Nanotechnol.* **4**, 562–566 (2009).
- [77] Tapasztó, L. *et al.* Breakdown of continuum mechanics for nanometre-wavelength rippling of graphene. *Nat. Phys.* **8**, 739–742 (2012).
- [78] Choi, J. S. *et al.* Friction Anisotropy-Driven Domain Imaging on Exfoliated Monolayer Graphene. *Science* **333**, 607–610 (2011).
- [79] Lee, J. H. *et al.* Universality of strain-induced anisotropic friction domains on 2D materials. *NPG Asia Mater.* **10**, 1069–1075 (2018).
- [80] Gallagher, P. *et al.* Switchable friction enabled by nanoscale self-assembly on graphene. *Nat. Commun.* **7**, 10745 (2016).
- [81] Almeida, C. M. *et al.* Giant and Tunable Anisotropy of Nanoscale Friction in Graphene. *Sci. Rep.* **6**, 31569 (2016).
- [82] Cao, X. *et al.* Anisotropic nanofriction on MoS₂ with different thicknesses. *Tribol. Int.* **134**, 308–316 (2019).
- [83] Baykara, M. Z. & Schwarz, U. D. Atomic Force Microscopy: Methods and Applications. in *Encyclopedia of Spectroscopy and Spectrometry* 70–75 (Elsevier, 2017). doi:10.1016/B978-0-12-409547-2.12141-9.
- [84] García, R. *Amplitude Modulation Atomic Force Microscopy*. (Wiley-VCH, 2010). doi:10.1002/9783527632183.

- [85] Albrecht, T. R., Grütter, P., Horne, D. & Rugar, D. Frequency modulation detection using high- Q cantilevers for enhanced force microscope sensitivity. *J. Appl. Phys.* **69**, 668–673 (1991).
- [86] Kumar, C. S. S. R. *Surface Science Tools for Nanomaterials Characterization. Surface Science Tools for Nanomaterials Characterization* (Springer Berlin Heidelberg, 2015). doi:10.1007/978-3-662-44551-8.
- [87] Albers, B. J. *et al.* Three-dimensional imaging of short-range chemical forces with picometre resolution. *Nat. Nanotechnol.* **4**, 307–310 (2009).
- [88] Sader, J. E. & Jarvis, S. P. Accurate formulas for interaction force and energy in frequency modulation force spectroscopy. *Appl. Phys. Lett.* **84**, 1801–1803 (2004).
- [89] Dagdeviren, O. E., Zhou, C., Altman, E. I. & Schwarz, U. D. Quantifying Tip-Sample Interactions in Vacuum Using Cantilever-Based Sensors: An Analysis. *Phys. Rev. Appl.* **9**, 044040 (2018).
- [90] Sader, J. E., Hughes, B. D., Huber, F. & Giessibl, F. J. Interatomic force laws that evade dynamic measurement. *Nat. Nanotechnol.* **13**, 1088–1091 (2018).
- [91] Li, J., Li, J., Jiang, L. & Luo, J. Fabrication of a graphene layer probe to measure force interactions in layered heterojunctions. *Nanoscale* **12**, 5435–5443 (2020).
- [92] Fang, L. *et al.* Thickness dependent friction on few-layer MoS₂, WS₂, and WSe₂. *Nanotechnology* **28**, 245703 (2017).
- [93] Quereda, J., Castellanos-Gomez, A., Agraït, N. & Rubio-Bollinger, G. Single-layer MoS₂ roughness and sliding friction quenching by interaction with atomically flat substrates. *Appl. Phys. Lett.* **105**, 053111 (2014).
- [94] Lee, H. *et al.* Nanoscale Friction on Confined Water Layers Intercalated between MoS₂ Flakes and Silica. *J. Phys. Chem. C* **123**, 8827–8835 (2019).
- [95] Jacobs, T. D. B., Wabiszewski, G. E., Goodman, A. J. & Carpick, R. W. Characterizing nanoscale scanning probes using electron microscopy: A novel fixture and a practical guide. *Rev. Sci. Instrum.* **87**, 013703 (2016).